# Unravelling the complex speciation of halozincate ionic liquids using X-ray spectroscopies and calculations

J. M. Seymour,[1] E. Gousseva,[1] F. K. Towers Tompkins,[1] L. G. Parker,[1] N. O. Alblewi,[1] C. J Clarke,[2] S. Hayama,[3] R. G. Palgrave,[4] R. A. Bennett,[1] R. P. Matthews,*[5] K. R. J. Lovelock*[1]

[1] Department of Chemistry, University of Reading, Reading, UK
[2] School of Chemistry, University of Nottingham, Nottingham, UK
[3] Diamond Light Source, Harwell, UK
[4] Department of Chemistry, University College London, UK
[5] School of Health, Sport and Bioscience, University of East London, UK
* k.r.j.lovelock@reading.ac.uk
* R.Matthews3@uel.ac.uk

1. Ionic Liquids Studied and Synthesis S2-S6
2. Data analysis. Peak fitting core level XP spectra and charge referencing S7-S8
3. Calculations: anions studied S9
4. Calculations: producing calculated XP spectra and calculated XANES spectra S10-S11
5. Results. XPS: demonstrating purity S12-S32
6. Results. XPS: $E_B$(core) S33
7. Results. XPS: Core S34-S35
8. Results. XPS: FWHM S36-S38
9. Results. XPS: Valence S39
10. Results. Calculations: total energies for gas phase calculations S40
11. Results. XPS: halometallates with one halide electronic environment S41-S42
12. Results. Effect of basis set on calculated Cl 2p XPS S43
13. Results. Effect of solvation environment on calculated Cl 2p XPS S44
14. References S45

## 1. Ionic Liquids Studied and Synthesis

Table S1 gives the ionic liquids (ILs) studied. Core and valence XP spectra were published for 16 ILs in the ESI of reference [1] and for three ILs in the ESI of reference [2]. The synthesis for the $x$ = 0.43 IL was given in reference [3]. The XPS apparatus used for the new IL is described in reference [2]. All 20 ILs were liquid at room temperature, making XPS experiments relatively straightforward, as no heating was required for any IL studied here. For laboratory XPS measurements, the samples were mounted in air; exposure to air was limited to <10 minutes.

**Table S1.** ILs investigated in this work.

| IL no. | Abbreviation | Structure | Name | XPS first published |
|---|---|---|---|---|
| 1 | $[C_8C_1Im]Cl$ | 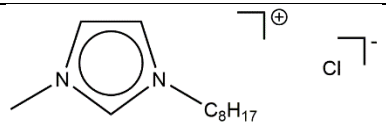 | 1–octyl–3–methylimidazolium chloride | [1] |
| 2 | $[C_8C_1Im]_2[ZnCl_4]$ | 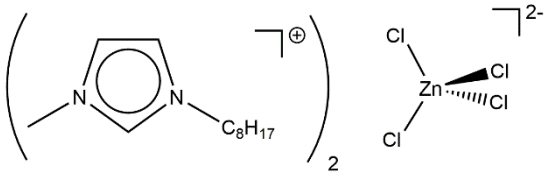 | bis(1-octyl-3-methylimidazolium) tetrachlorozincate | [1] |
| 3 | $[C_8C_1Im]_4[ZnCl_4][Zn_2Cl_6]$ | 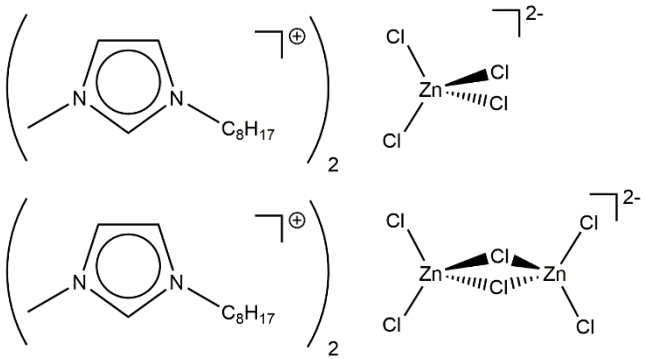 | bis(1-octyl-3-methylimidazolium) (tetrachlorozincate)(hexachlorodizincate) | here |
| 4 | $[C_8C_1Im]_2[Zn_2Cl_6]$ | 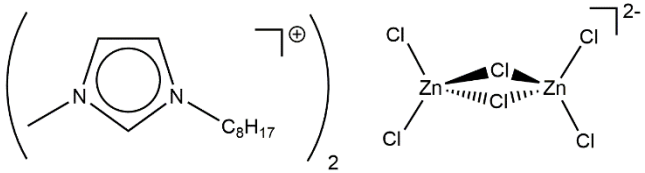 | bis(1-octyl-3-methylimidazolium) hexachlorodizincate | [1] |
| 5 | $[C_8C_1Im]_2[Zn_3Cl_8]$ | 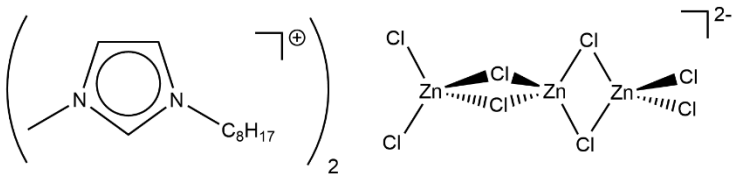 | bis(1-octyl-3-methylimidazolium) octachlorootrizincate | [2] |

| | | | | | |
|---|---|---|---|---|---|
| 6 | $[C_8C_1Im]_2[Zn_4Cl_{10}]$ | 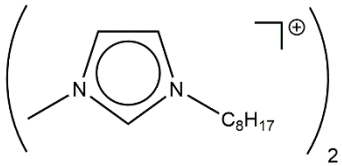 | 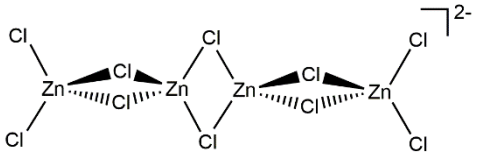 | bis(1-octyl-3-methylimidazolium) decachlorotetrazincate [a] | 1 |
| 7 | $[C_8C_1Im]Br$ | 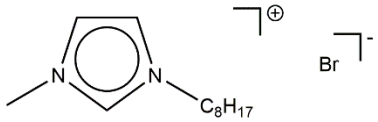 | | 1–octyl–3–methylimidazolium bromide | 1 |
| 8 | $[C_8C_1Im]_2[ZnBr_4]$ | 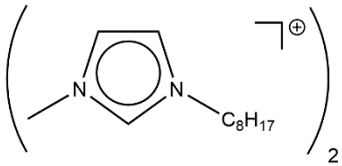 | 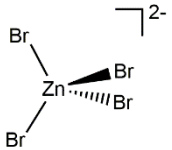 | bis(1-octyl-3-methylimidazolium) tetrabromozincate | 1 |
| 9 | $[C_8C_1Im]_2[Zn_2Br_6]$ | 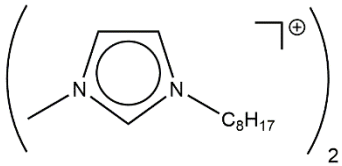 | 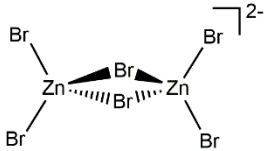 | bis(1-octyl-3-methylimidazolium) hexabromodizincate | 1 |
| 10 | $[C_8C_1Im]_2[Zn_3Br_8]$ | 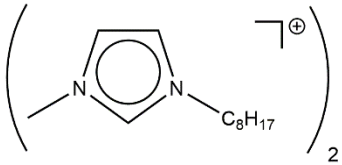 | 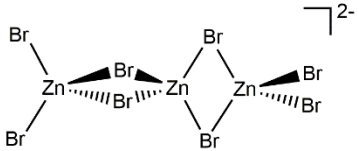 | bis(1-octyl-3-methylimidazolium) octabromotrizincate | 1 |
| 11 | $[C_8C_1Im]_2[Zn_4Br_{10}]$ | 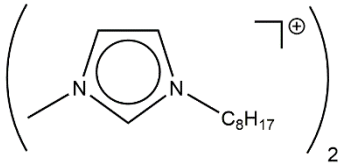 | 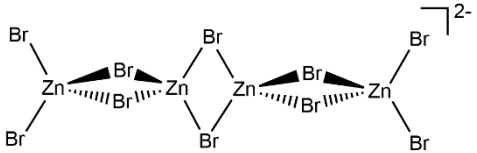 | bis(1-octyl-3-methylimidazolium) decabromotetrazincate [a] | 1 |

| | | | | |
|---|---|---|---|---|
| 12 | $[P_{6,6,6,14}]_2[ZnCl_4]$ | 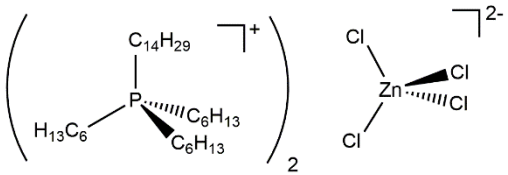 | tetradecyl(trihexyl)phosphonium tetrachlorozincate | 1 |
| 13 | $[C_8C_1Im]_2[FeCl_4]$ | 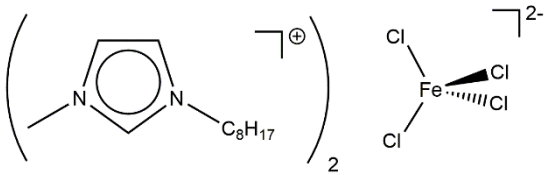 | bis(1-octyl-3-methylimidazolium) tetrachloroferrate | 1 |
| 14 | $[C_8C_1Im]_2[CoCl_4]$ | 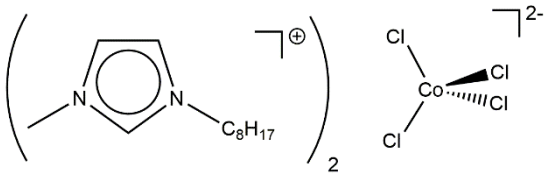 | bis(1-octyl-3-methylimidazolium) tetrachlorocobaltate | 1 |
| 15 | $[C_8C_1Im]_2[NiCl_4]$ | 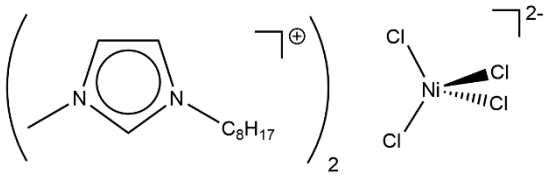 | bis(1-octyl-3-methylimidazolium) tetrachloronickelate | 1 |
| 16 | $[C_8C_1Im]_2[CoBr_4]$ | 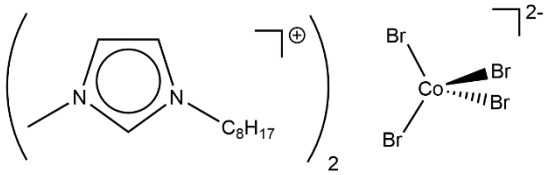 | bis(1-octyl-3-methylimidazolium) tetrabromocobaltate | 1 |
| 17 | $[C_8C_1Im][SnCl_3]$ | 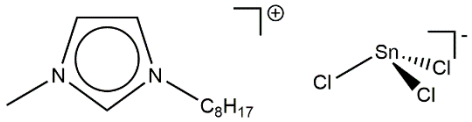 | 1-octyl-3-methylimidazolium trichlorostannate | 1 |
| 18 | $[C_8C_1Im][InCl_4]$ | 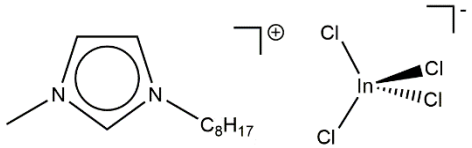 | 1-octyl-3-methylimidazolium tetrachloroindate | 1 |

| | | | | |
|---|---|---|---|---|
| 19 | $[C_8C_1Im][SnBr_3]$ | 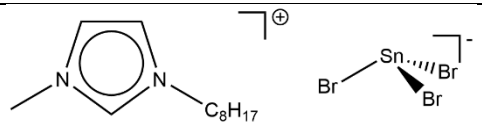 | 1-octyl-3-methylimidazolium tribromostannate | 2 |
| 20 | $[C_8C_1Im][InBr_4]$ | 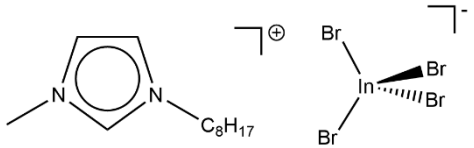 | 1-octyl-3-methylimidazolium tetrabromoindate | 2 |

[a] $[Zn_4Cl_{10}]^{2-}$ and $[Zn_4Br_{10}]^{2-}$ drawn as linear, but supertetrahedron ring will also be present

## 2. Data analysis. Peak fitting core level XP spectra and charge referencing

Peak fitting core level XP spectra is important for demonstrating purity (ESI Section 5). For this work peak fitting core level XP spectra is equally important for charge referencing. $E_B(C_{alkyl}\ 1s)$ was used for charge referencing all 20 ILs. The constraints used were all explained in the ESI of reference [4].

Fitting core level XP spectra: C 1s and N 1s

Fitting for C 1s and N 1s XPS for the cations studied here, $[C_8C_1Im]^+$ and $[P_{6,6,6,14}]^+$, were given in detail in reference [4] and are summarised in Table S2.

Fitting core level XP spectra: spin-orbit coupling

For halozincate anions, three elements gave spin-orbit coupling that required fitting constraints to be used: Cl 2p, Br 3d. $\Delta E_B$(Cl $2p_{3/2}$ - Cl $2p_{3/2}$) = 1.60 eV and the peak area ratio for Cl $2p_{3/2}$ to Cl $2p_{3/2}$ is 2:1. $\Delta E_B$(Br $3d_{5/2}$ - Br $3d_{3/2}$) = 1.04 eV and the peak area ratio for Br $3d_{5/2}$ to Br $3d_{3/2}$ is 3:2. Given that peaks due to Zn $2p_{3/2}$ and Zn $2p_{1/2}$ are very well separated (~23.07 eV), no fitting constraints were required.

Fitting core level XP spectra: Cl 2p for $x$ = 0.43

The predicted speciation for $x$ = 0.43 is $[C_8C_1Im]_4[ZnCl_4][Zn_2Cl_6]$. For the Cl 2p XP spectrum for $x$ = 0.43, a number of different constraints give acceptable fits. As there appears to be one Cl electronic environment and a shoulder at higher $E_B$, we constrained the fit to be eight $Cl_{terminal}$ to two $Cl_{bridging}$; even then, to obtain a reasonable fit all four component FWHM had to fixed as the same (ESI Table S2).

**Table S2.** Fitting constraints used for core level X-ray photoelectron spectroscopy (XPS) for each ionic liquid

| IL no. | IL | Core level | Fitting constraints used |
|---|---|---|---|
| 1 | $[C_8C_1Im]Cl$ | C 1s | Peak area ratio 1:4:7 for $C^2$:$C_{hetero}$:$C_{alkyl}$ |
| | | Cl 2p | Peak area ratio 1:2 for $2p_{1/2}$:$2p_{3/2}$<br>$\Delta E_B$(Cl $2p_{3/2}$ - Cl $2p_{3/2}$) = 1.60 eV |
| 2 | $[C_8C_1Im]_2[ZnCl_4]$ | C 1s | Peak area ratio 1:4:7 for $C^2$:$C_{hetero}$:$C_{alkyl}$ |
| | | Cl 2p | Peak area ratio 1:2 for $2p_{1/2}$:$2p_{3/2}$<br>$\Delta E_B$(Cl $2p_{3/2}$ - Cl $2p_{3/2}$) = 1.60 eV |
| 3 | $[C_8C_1Im]_4[ZnCl_4][Zn_2Cl_6]$ | C 1s | Peak area ratio 1:4:7 for $C^2$:$C_{hetero}$:$C_{alkyl}$ |
| | | Cl 2p | Peak area ratio 1:2 for $2p_{1/2}$:$2p_{3/2}$<br>Peak area ratio 1:4 for $Cl_{bridging}$:$Cl_{terminal}$<br>$\Delta E_B$(Cl $2p_{3/2}$ - Cl $2p_{3/2}$) = 1.60 eV<br>FWHM($Cl_{terminal}$ $2p_{3/2}$) = FWHM($Cl_{terminal}$ $2p_{1/2}$) =<br>FWHM($Cl_{bridging}$ $2p_{3/2}$) = FWHM($Cl_{bridging}$ $2p_{1/2}$) |
| 4 | $[C_8C_1Im]_2[Zn_2Cl_6]$ | C 1s | Peak area ratio 1:4:7 for $C^2$:$C_{hetero}$:$C_{alkyl}$ |
| | | Cl 2p | Peak area ratio 1:2 for $2p_{1/2}$:$2p_{3/2}$<br>Peak area ratio 1:2 for $Cl_{bridging}$:$Cl_{terminal}$<br>$\Delta E_B$(Cl $2p_{3/2}$ - Cl $2p_{3/2}$) = 1.60 eV<br>FWHM($Cl_{terminal}$ $2p_{3/2}$) = FWHM($Cl_{terminal}$ $2p_{1/2}$)<br>FWHM($Cl_{bridging}$ $2p_{3/2}$) = FWHM($Cl_{bridging}$ $2p_{1/2}$) |
| 5 | $[C_8C_1Im]_2[Zn_3Cl_8]$ | C 1s | Peak area ratio 1:4:7 for $C^2$:$C_{hetero}$:$C_{alkyl}$ |
| | | Cl 2p | Peak area ratio 1:2 for $2p_{1/2}$:$2p_{3/2}$<br>Peak area ratio 1:1 for $Cl_{bridging}$:$Cl_{terminal}$<br>$\Delta E_B$(Cl $2p_{3/2}$ - Cl $2p_{3/2}$) = 1.60 eV<br>FWHM($Cl_{terminal}$ $2p_{3/2}$) = FWHM($Cl_{terminal}$ $2p_{1/2}$)<br>FWHM($Cl_{bridging}$ $2p_{3/2}$) = FWHM($Cl_{bridging}$ $2p_{1/2}$) |
| 6 | $[C_8C_1Im]_2[Zn_4Cl_{10}]$ | C 1s | Peak area ratio 1:4:7 for $C^2$:$C_{hetero}$:$C_{alkyl}$ |
| | | Cl 2p | Peak area ratio 1:2 for $2p_{1/2}$:$2p_{3/2}$<br>Peak area ratio 3:2 for $Cl_{bridging}$:$Cl_{terminal}$<br>$\Delta E_B$(Cl $2p_{3/2}$ - Cl $2p_{3/2}$) = 1.60 eV<br>FWHM($Cl_{terminal}$ $2p_{3/2}$) = FWHM($Cl_{terminal}$ $2p_{1/2}$)<br>FWHM($Cl_{bridging}$ $2p_{3/2}$) = FWHM($Cl_{bridging}$ $2p_{1/2}$) |
| 7 | $[C_8C_1Im]Br$ | C 1s | Peak area ratio 1:4:7 for $C^2$:$C_{hetero}$:$C_{alkyl}$ |
| | | Br 3d | Peak area ratio 2:3 for $3d_{3/2}$:$3d_{5/2}$ |

| | | | |
|---|---|---|---|
| | | | $\Delta E_B$(Br $3d_{5/2}$ - Br $3d_{3/2}$) = 1.04 eV |
| 8 | $[C_8C_1Im]_2[ZnBr_4]$ | C 1s<br>Br 3d | Peak area ratio 1:4:7 for $C^2$:$C_{hetero}$:$C_{alkyl}$<br>Peak area ratio 2:3 for $3d_{3/2}$:$3d_{5/2}$<br>$\Delta E_B$(Br $3d_{5/2}$ - Br $3d_{3/2}$) = 1.04 eV |
| 9 | $[C_8C_1Im]_2[Zn_2Br_6]$ | C 1s<br>Br 3d | Peak area ratio 1:4:7 for $C^2$:$C_{hetero}$:$C_{alkyl}$<br>Peak area ratio 2:3 for $3d_{3/2}$:$3d_{5/2}$<br>Peak area ratio 1:2 for $Br_{bridging}$:$Br_{terminal}$<br>$\Delta E_B$(Br $3d_{5/2}$ - Br $3d_{3/2}$) = 1.04 eV<br>FWHM($Br_{terminal}$ $3d_{5/2}$) = FWHM($Br_{terminal}$ $3d_{3/2}$)<br>FWHM($Br_{bridging}$ $3d_{5/2}$) = FWHM($Br_{bridging}$ $3d_{3/2}$) |
| 10 | $[C_8C_1Im]_2[Zn_3Br_8]$ | C 1s<br>Br 3d | Peak area ratio 1:4:7 for $C^2$:$C_{hetero}$:$C_{alkyl}$<br>Peak area ratio 2:3 for $3d_{3/2}$:$3d_{5/2}$<br>Peak area ratio 1:1 for $Br_{bridging}$:$Br_{terminal}$<br>$\Delta E_B$(Br $3d_{5/2}$ - Br $3d_{3/2}$) = 1.04 eV<br>FWHM($Br_{terminal}$ $3d_{5/2}$) = FWHM($Br_{terminal}$ $3d_{3/2}$)<br>FWHM($Br_{bridging}$ $3d_{5/2}$) = FWHM($Br_{bridging}$ $3d_{3/2}$) |
| 11 | $[C_8C_1Im]_2[Zn_4Br_{10}]$ | C 1s<br>Br 3d | Peak area ratio 1:4:7 for $C^2$:$C_{hetero}$:$C_{alkyl}$<br>Peak area ratio 2:3 for $3d_{3/2}$:$3d_{5/2}$<br>Peak area ratio 3:2 for $Br_{bridging}$:$Br_{terminal}$<br>$\Delta E_B$(Br $3d_{5/2}$ - Br $3d_{3/2}$) = 1.04 eV<br>FWHM($Br_{terminal}$ $3d_{5/2}$) = FWHM($Br_{terminal}$ $3d_{3/2}$)<br>FWHM($Br_{bridging}$ $3d_{5/2}$) = FWHM($Br_{bridging}$ $3d_{3/2}$) |
| 12 | $[P_{6,6,6,14}]_2[ZnCl_4]$ | C 1s<br>Cl 2p<br>P 2p | Peak area ratio 4:28 for $C_{hetero}$:$C_{alkyl}$<br>FWHM($C_{hetero}$) = FWHM($C_{alkyl}$)<br>Peak area ratio 1:2 for $2p_{1/2}$:$2p_{3/2}$<br>$\Delta E_B$(Cl $2p_{3/2}$ - Cl $2p_{3/2}$) = 1.60 eV<br>Peak area ratio 1:2 for $2p_{1/2}$:$2p_{3/2}$ |
| 13 | $[C_8C_1Im]_2[FeCl_4]$ | C 1s<br>Cl 2p | Peak area ratio 1:4:7 for $C^2$:$C_{hetero}$:$C_{alkyl}$<br>Peak area ratio 1:2 for $2p_{1/2}$:$2p_{3/2}$<br>$\Delta E_B$(Cl $2p_{3/2}$ - Cl $2p_{3/2}$) = 1.60 eV |
| 14 | $[C_8C_1Im]_2[CoCl_4]$ | C 1s<br>Cl 2p | Peak area ratio 1:4:7 for $C^2$:$C_{hetero}$:$C_{alkyl}$<br>1:2 for $2p_{1/2}$:$2p_{3/2}$<br>$\Delta E_B$(Cl $2p_{3/2}$ - Cl $2p_{3/2}$) = 1.60 eV |
| 15 | $[C_8C_1Im]_2[NiCl_4]$ | C 1s<br>Cl 2p | Peak area ratio 1:4:7 for $C^2$:$C_{hetero}$:$C_{alkyl}$<br>Peak area ratio 1:2 for $2p_{1/2}$:$2p_{3/2}$<br>$\Delta E_B$(Cl $2p_{3/2}$ - Cl $2p_{3/2}$) = 1.60 eV |
| 16 | $[C_8C_1Im]_2[CoBr_4]$ | C 1s<br>Br 3d | Peak area ratio 1:4:7 for $C^2$:$C_{hetero}$:$C_{alkyl}$<br>Peak area ratio 2:3 for $3d_{3/2}$:$3d_{5/2}$<br>$\Delta E_B$(Br $3d_{5/2}$ - Br $3d_{3/2}$) = 1.04 eV |
| 17 | $[C_8C_1Im][SnCl_3]$ | C 1s<br>Cl 2p | Peak area ratio 1:4:7 for $C^2$:$C_{hetero}$:$C_{alkyl}$<br>Peak area ratio 1:2 for $2p_{1/2}$:$2p_{3/2}$<br>$\Delta E_B$(Cl $2p_{3/2}$ - Cl $2p_{3/2}$) = 1.60 eV |
| 18 | $[C_8C_1Im][InCl_4]$ | C 1s<br>Cl 2p | Peak area ratio 1:4:7 for $C^2$:$C_{hetero}$:$C_{alkyl}$<br>Peak area ratio 1:2 for $2p_{1/2}$:$2p_{3/2}$<br>$\Delta E_B$(Cl $2p_{3/2}$ - Cl $2p_{3/2}$) = 1.60 eV |
| 19 | $[C_8C_1Im][SnBr_3]$ | C 1s<br>Br 3d | Peak area ratio 1:4:7 for $C^2$:$C_{hetero}$:$C_{alkyl}$<br>Peak area ratio 2:3 for $3d_{3/2}$:$3d_{5/2}$<br>$\Delta E_B$(Br $3d_{5/2}$ - Br $3d_{3/2}$) = 1.04 eV |
| 20 | $[C_8C_1Im][InBr_4]$ | C 1s<br>Br 3d | Peak area ratio 1:4:7 for $C^2$:$C_{hetero}$:$C_{alkyl}$<br>Peak area ratio 2:3 for $3d_{3/2}$:$3d_{5/2}$<br>$\Delta E_B$(Br $3d_{5/2}$ - Br $3d_{3/2}$) = 1.04 eV |

## 3. Calculations: anions studied

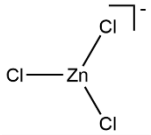


$[ZnCl_3]^-$

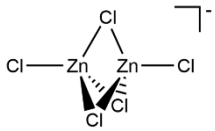


$[Zn_2Cl_5]^-$

**Figure S1.** -1 halometallate anions calculated.

## 4. Calculations: producing calculated XP spectra and calculated XANES spectra

To produce calculated XP spectra for orbitals that have spin-orbit coupling (Cl 2p, Br 3d, Zn 2p), each calculated $E_B$ value was adjusted using $E_B$ and area factors are given in ESI Table S3. Once the adjusted calculated $E_B$ were obtained, a Gaussian-Lorentzian Product (GLP) function was applied to each calculated $E_B$ data point for each core-state using Equation 1 and then summed to produce calculated XPS data. The mixing parameter, *m,* and function width, *F*, were set to the values given in Table S3.

To produce calculated XP spectra for orbitals that do not have spin-orbit coupling (in this article, valence XPS), a Gaussian-Lorentzian Product (GLP) function was applied to each calculated $E_B$ data point for each valence-state using Equation 1 and then summed to produce calculated XPS data. The mixing parameter, *m,* and function width, *F*, were set to the values given in Table S3.

$$GLP\ (x; F, E, m) = \frac{exp\left[-4\ln 2(1-m)\frac{(x-E)^2}{F^2}\right]}{\left[1+4m\frac{(x-E)^2}{F^2}\right]} \qquad \text{(Equation 1)}$$

To produce calculated Zn 1s XANES spectra, a Gaussian-Lorentzian Product (GLP) function was applied to each calculated energy data point using Equation 1 and then summed to produce calculated Zn 1s XANES data. $m$ = 0.30 and $F$ = 2.5.

**Table S3.** Values used to produce calculated XP spectra

| Orbital | FWHM / eV | Gaussian-Lorentzian (GL) Product function | Spin-orbit coupling $\Delta E_B$ / eV | $E_B$(calc.) with spin-orbit coupling correction | Spin-orbit coupling peak area ratio | Peak area ratio |
|---|---|---|---|---|---|---|
| Cl 2p | 0.90 | GL(30) | $\Delta E_B$(Cl $2p_{3/2}$ - Cl $2p_{3/2}$) = 1.60 eV | $E_B$(Cl $2p_{3/2}$,calc.) = $E_B$(Cl 2p,calc.) – (1.60 × 2/3)<br>$E_B$(Cl $2p_{1/2}$,calc.) = $E_B$(Cl 2p,calc.) + (1.60 × 1/3) | 1:2 for $2p_{1/2}$:$2p_{3/2}$ | Area(Cl $2p_{3/2}$,calc.) = Area(Cl 2p,calc.) × 2/3<br>Area(Cl $2p_{1/2}$,calc.) = Area(Cl 2p,calc.) × 1/3 |
| Br 3d | 0.90 | GL(30) | $\Delta E_B$(Br $3d_{5/2}$ - Br $3d_{3/2}$) = 1.04 eV | $E_B$(Br $3d_{5/2}$,calc.) = $E_B$(Br 3d,calc.) – (1.04 × 3/5)<br>$E_B$(Br $3d_{3/2}$,calc.) = $E_B$(Br 3d,calc.) + (1.04 × 2/5) | 2:3 for $3d_{3/2}$:$3d_{5/2}$ | Area(Br $3d_{5/2}$,calc.) = Area(Br 3d,calc.) × 3/5<br>Area(Br $3d_{3/2}$,calc.) = Area(Br 3d,calc.) × 2/5 |
| Zn 2p | 1.15 | GL(70) | $\Delta E_B$(Zn $2p_{3/2}$ - Zn $2p_{3/2}$) = 23.07 eV | $E_B$(Zn $2p_{3/2}$,calc.) = $E_B$(Zn 2p,calc.) – (23.07 × 2/3)<br>$E_B$(Zn $2p_{1/2}$,calc.) = $E_B$(Zn 2p,calc.) + (23.07 × 1/3) | Not needed due to large $\Delta E_B$ | Not needed due to large $\Delta E_B$ |
| Valence | 0.90 | GL(30) | N/A | N/A | N/A | N/A |

## 5. Results. XPS: demonstrating purity

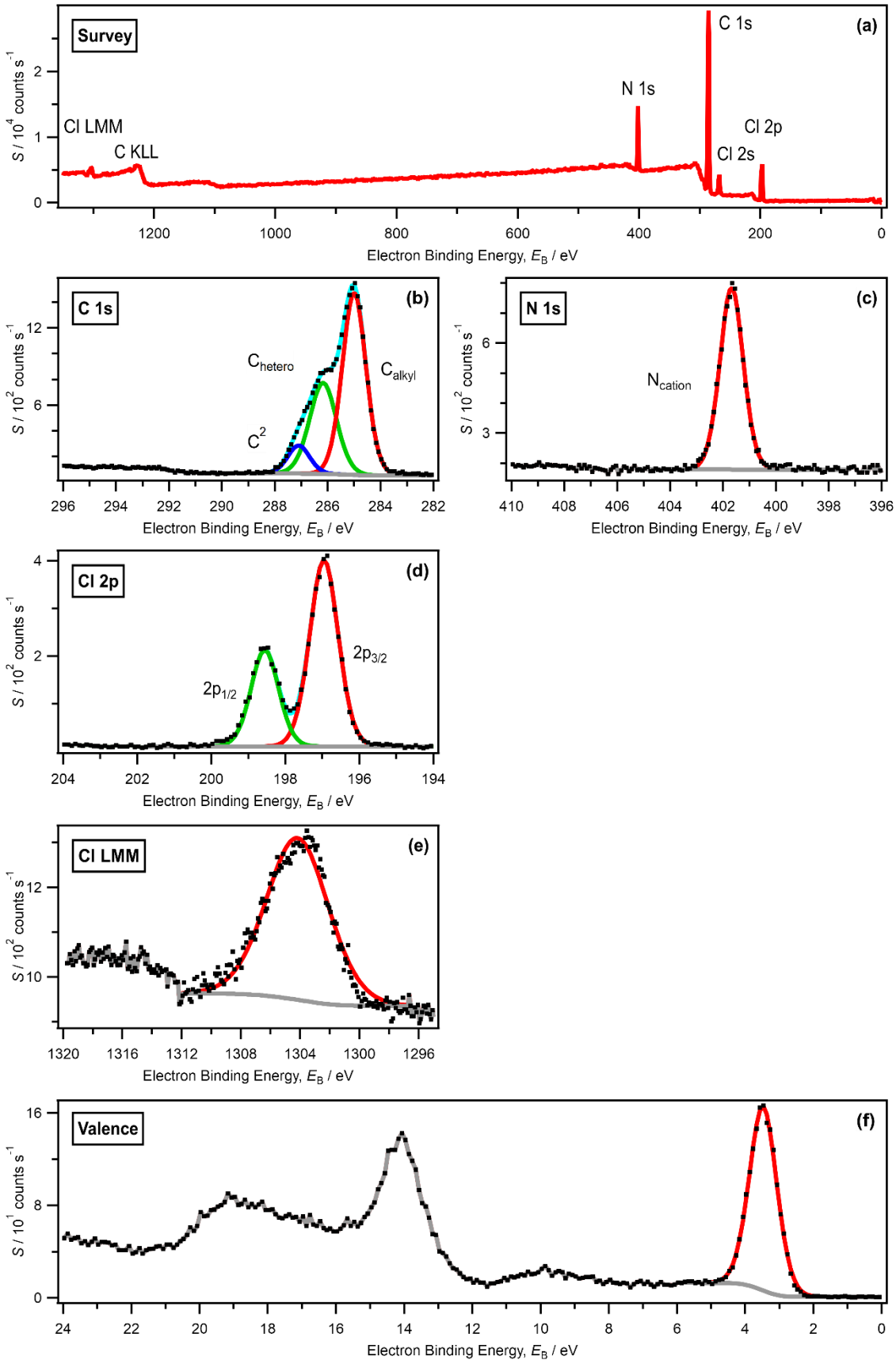


**Figure S2.** (a) Survey, (b-d) core, (e) Auger and (f) valence XP spectra for $[C_8C_1Im]Cl$ recorded on laboratory–based XPS apparatus at $h\nu$ = 1486.6 eV. All XP spectra were charge referenced using the method outlined in ESI Section 2.

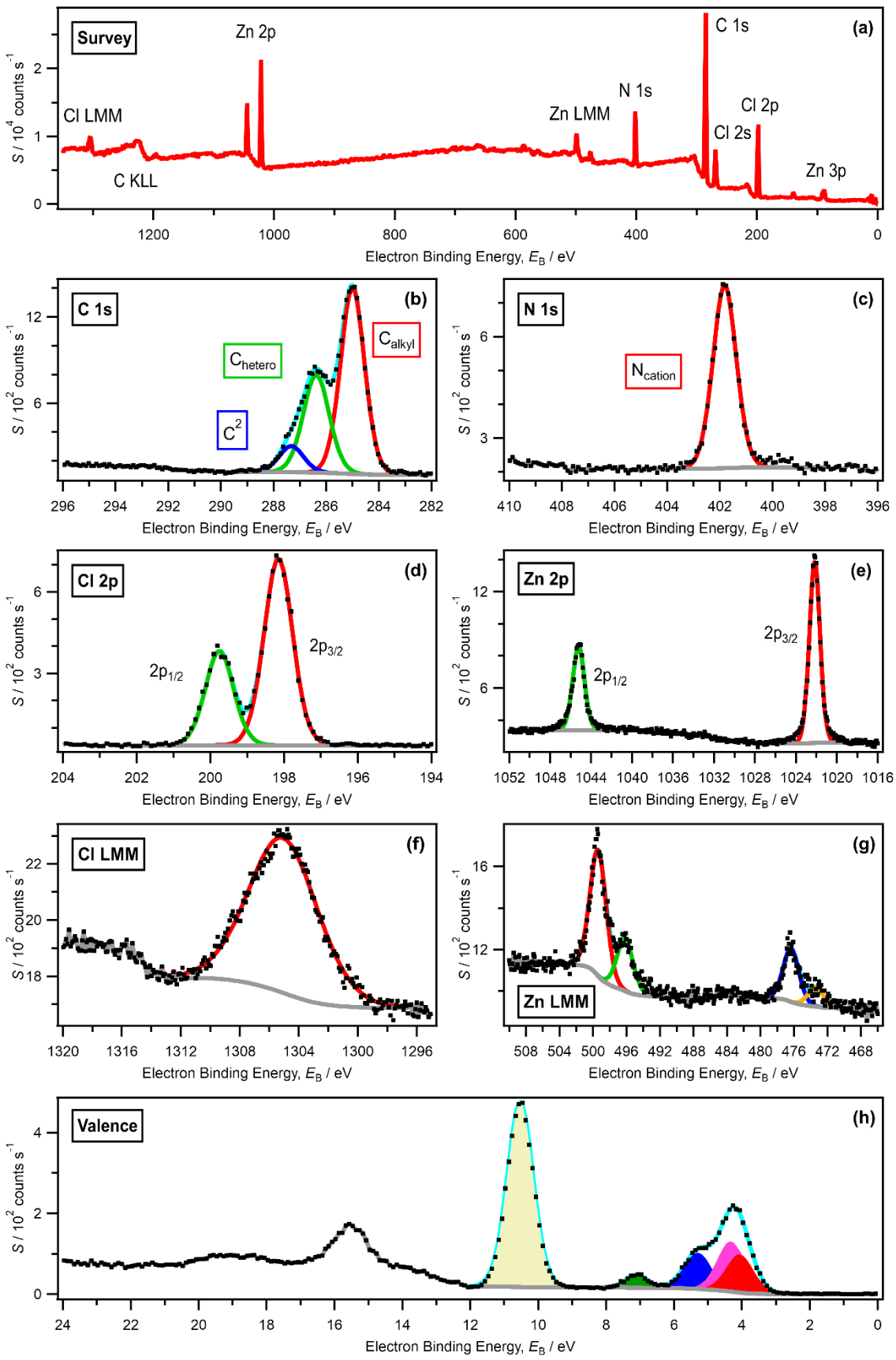


**Figure S3.** (a) Survey, (b-e) core, (f-g) Auger and (h) valence XP spectra for $[C_8C_1Im]_2[ZnCl_4]$ recorded on laboratory–based XPS apparatus at $h\nu$ = 1486.6 eV. All XP spectra were charge referenced using the method outlined in ESI Section 2.

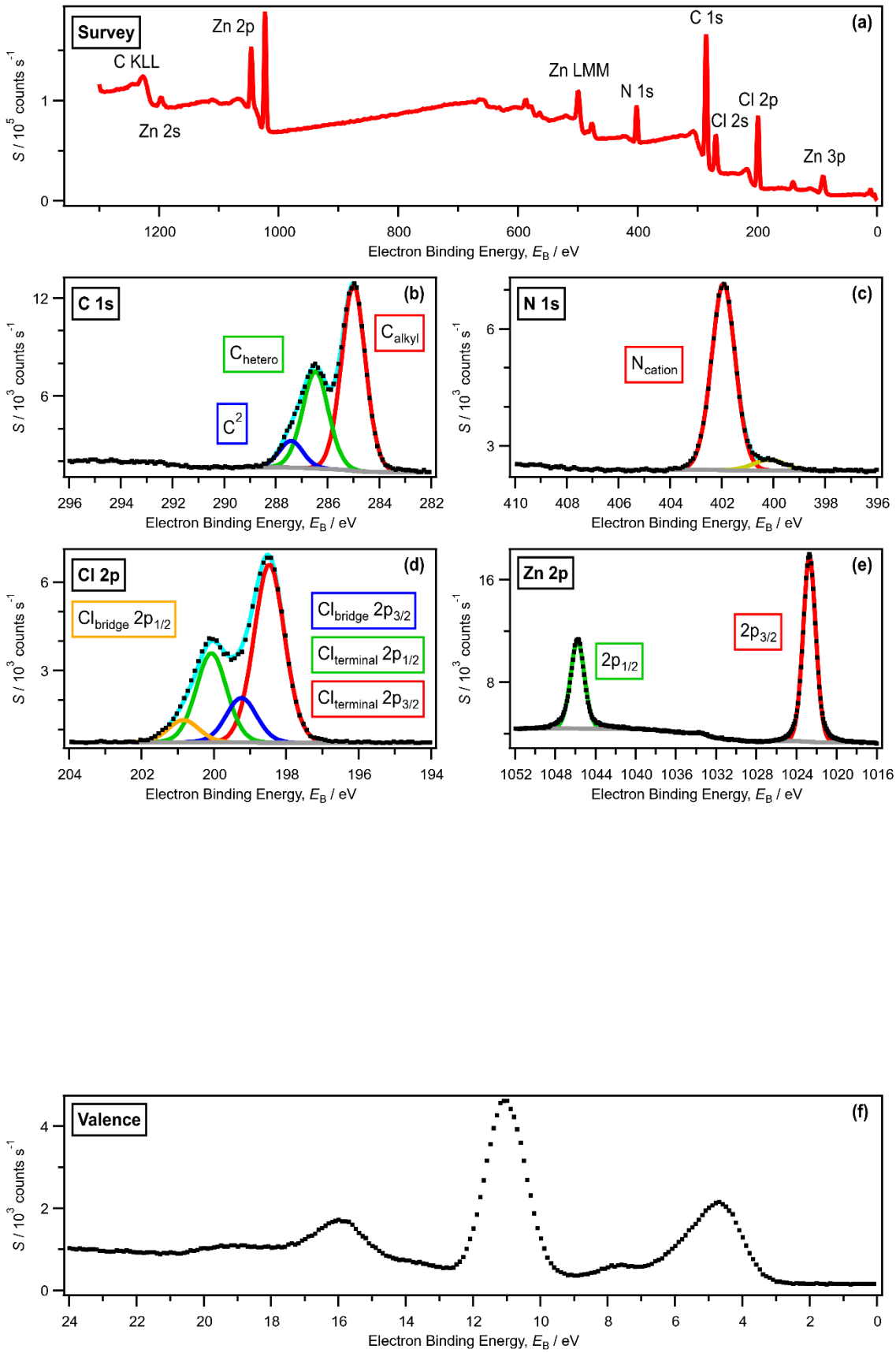


**Figure S4.** (a) Survey, (b-e) core and (f) valence XP spectra for $[C_8C_1Im]_4[ZnCl_4][Zn_2Cl_6]$ recorded on laboratory–based XPS apparatus at $h\nu$ = 1486.6 eV. All XP spectra were charge referenced using the method outlined in ESI Section 2.

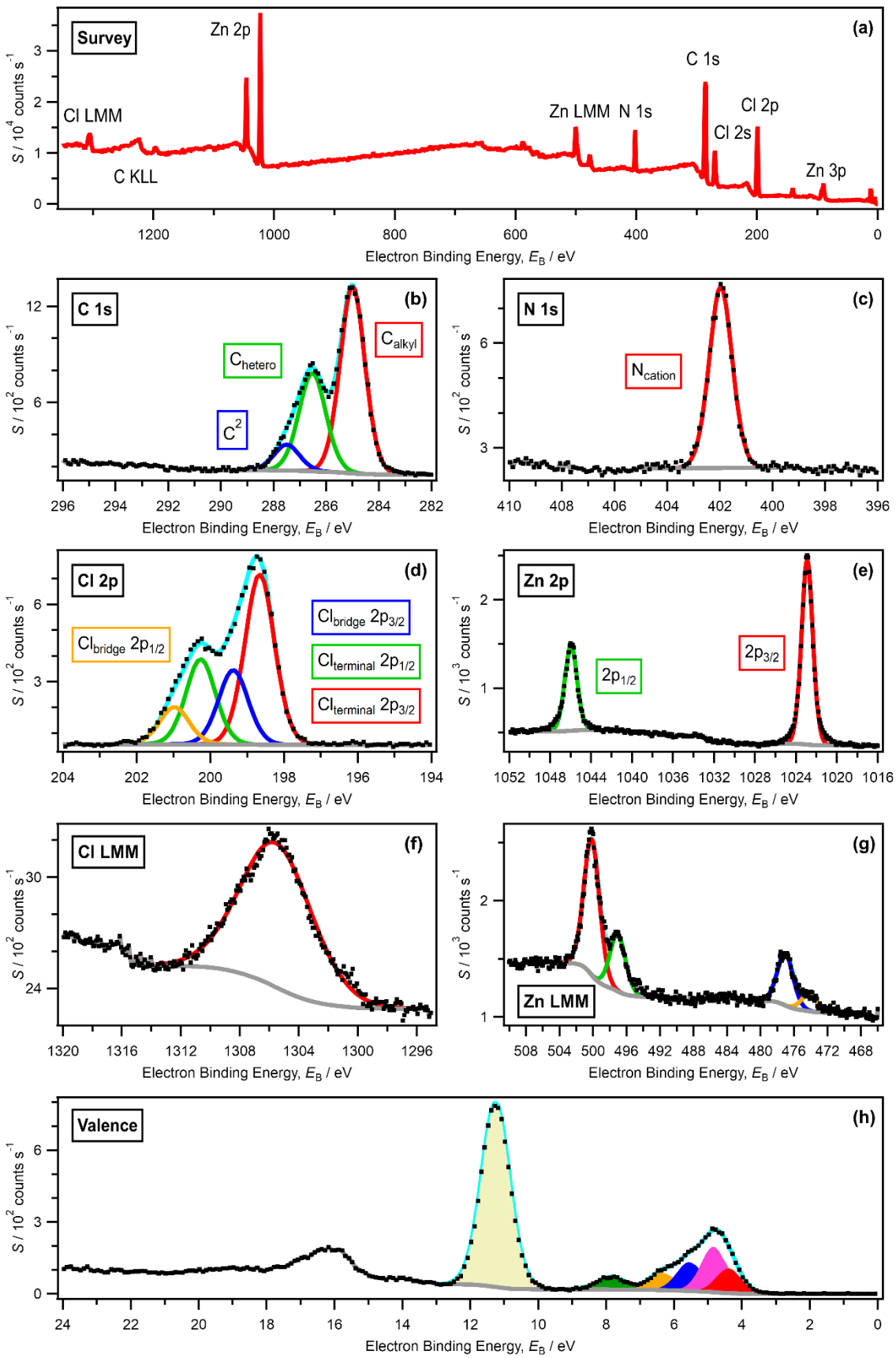


**Figure S5.** (a) Survey, (b-e) core, (f-g) Auger and (h) valence XP spectra for $[C_8C_1Im]_2[Zn_2Cl_6]$ recorded on laboratory–based XPS apparatus at $h\nu$ = 1486.6 eV. All XP spectra were charge referenced using the method outlined in ESI Section 2.

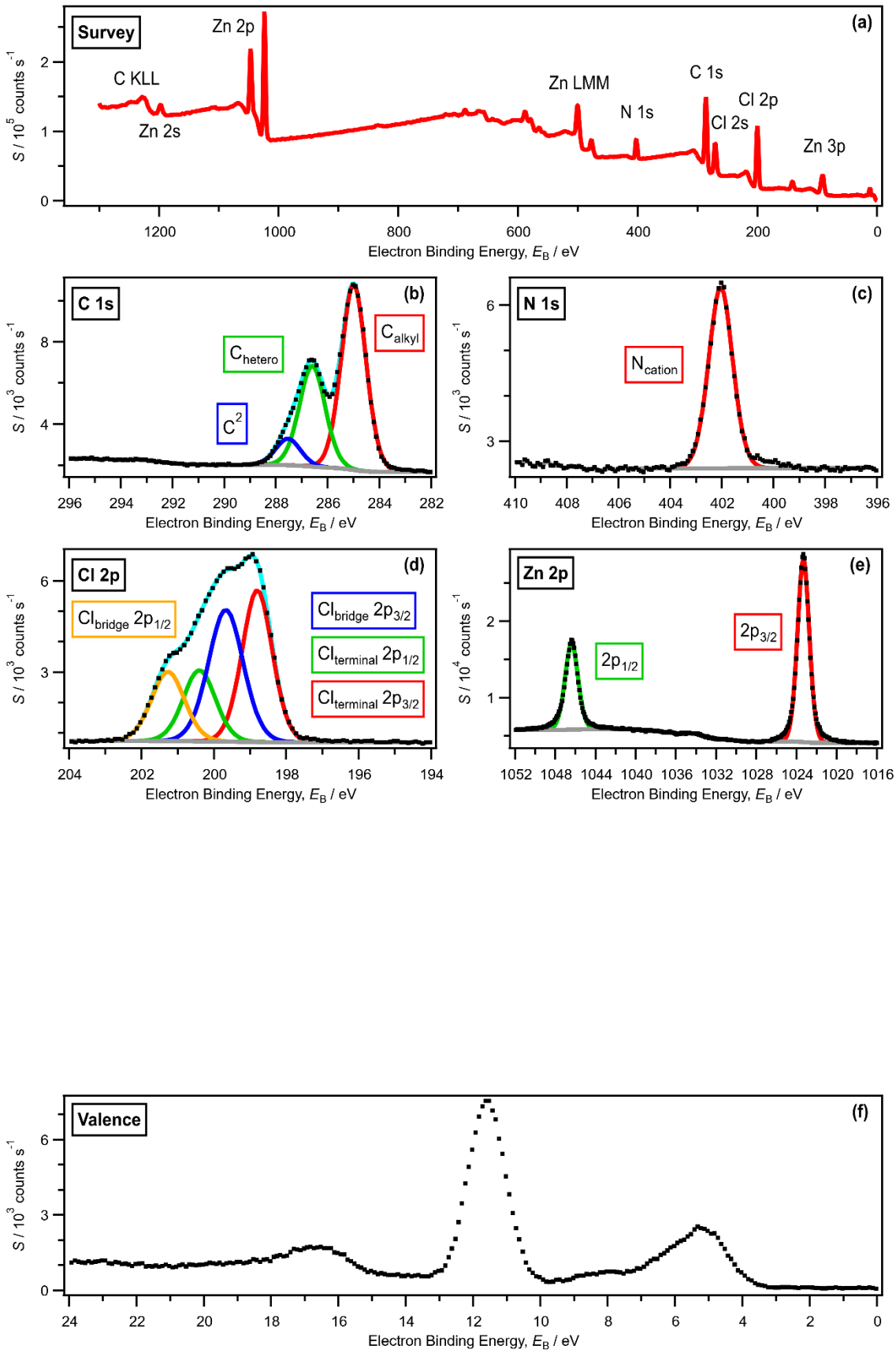


**Figure S6.** (a) Survey, (b-e) core and (f) valence XP spectra for $[C_8C_1Im]_2[Zn_3Cl_8]$ recorded on laboratory–based XPS apparatus at $h\nu$ = 1486.6 eV. All XP spectra were charge referenced using the method outlined in ESI Section 2.

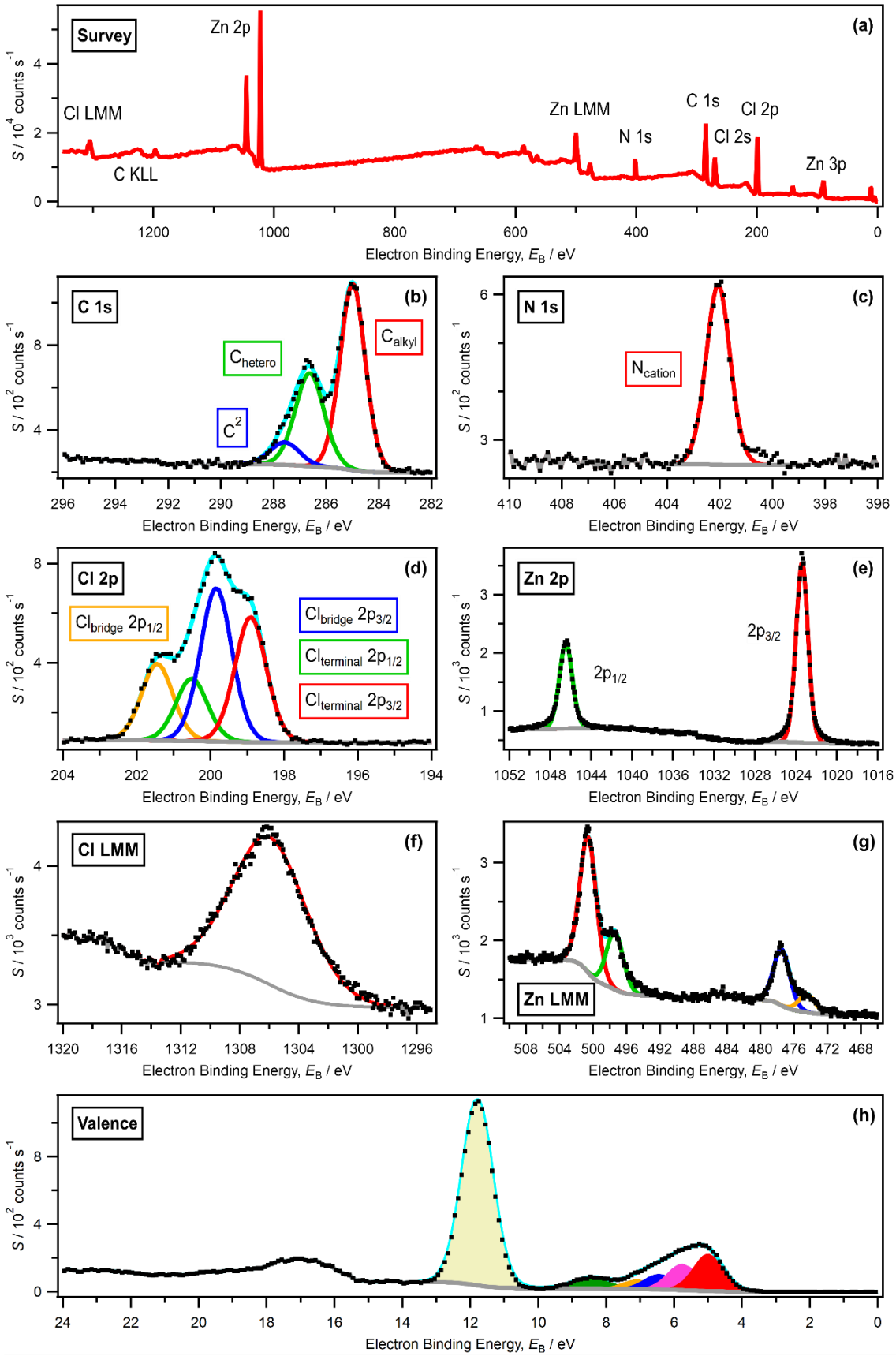


**Figure S7.** (a) Survey, (b-e) core, (f-g) Auger and (h) valence XP spectra for $[C_8C_1Im]_2[Zn_4Cl_{10}]$ recorded on laboratory–based XPS apparatus at $h\nu$ = 1486.6 eV. All XP spectra were charge referenced using the method outlined in ESI Section 2.

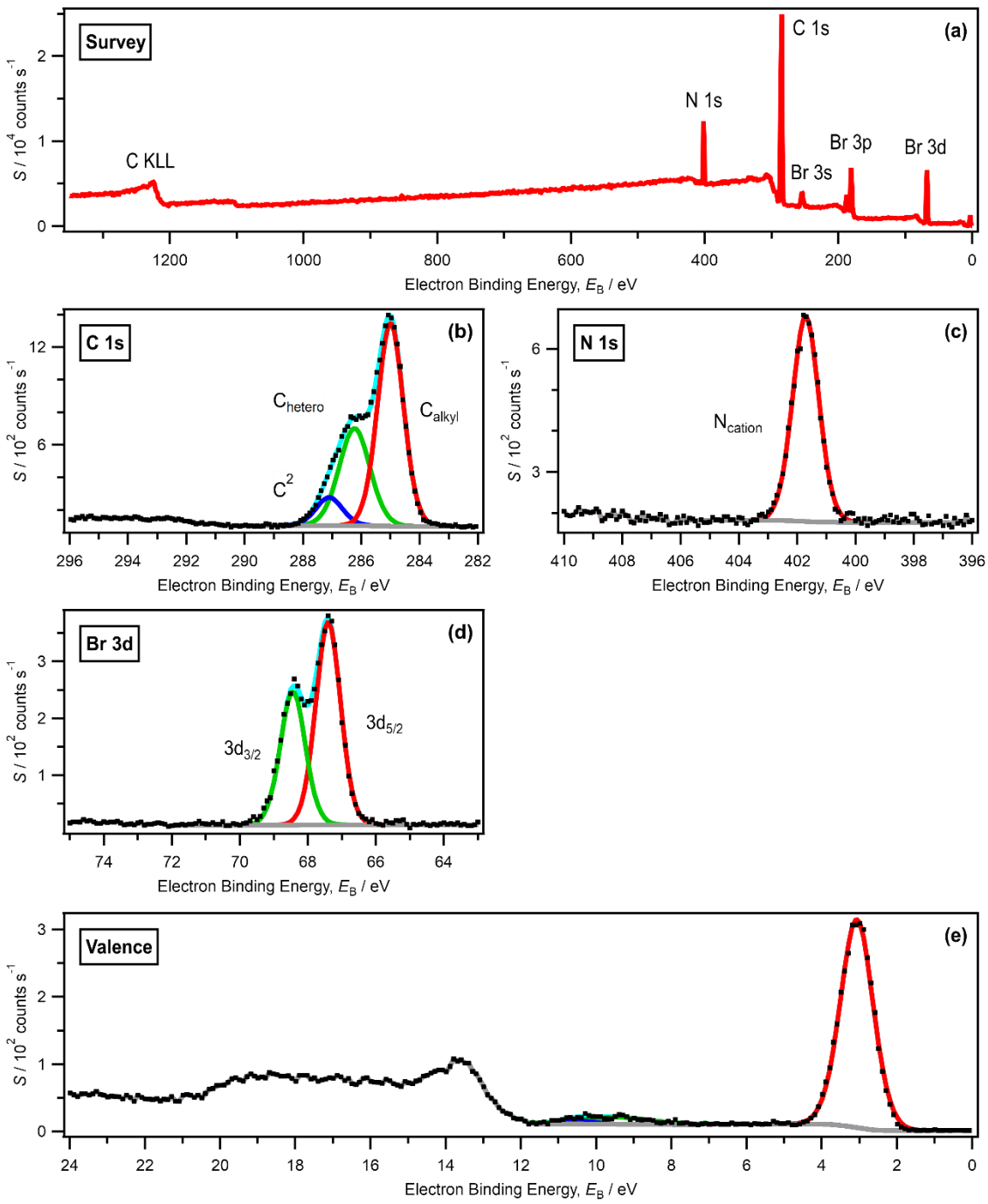


**Figure S8.** (a) Survey, (b-d) core and (e) valence XP spectra for $[C_8C_1Im]Br$ recorded on laboratory–based XPS apparatus at $h\nu$ = 1486.6 eV. All XP spectra were charge referenced using the method outlined in ESI Section 2.

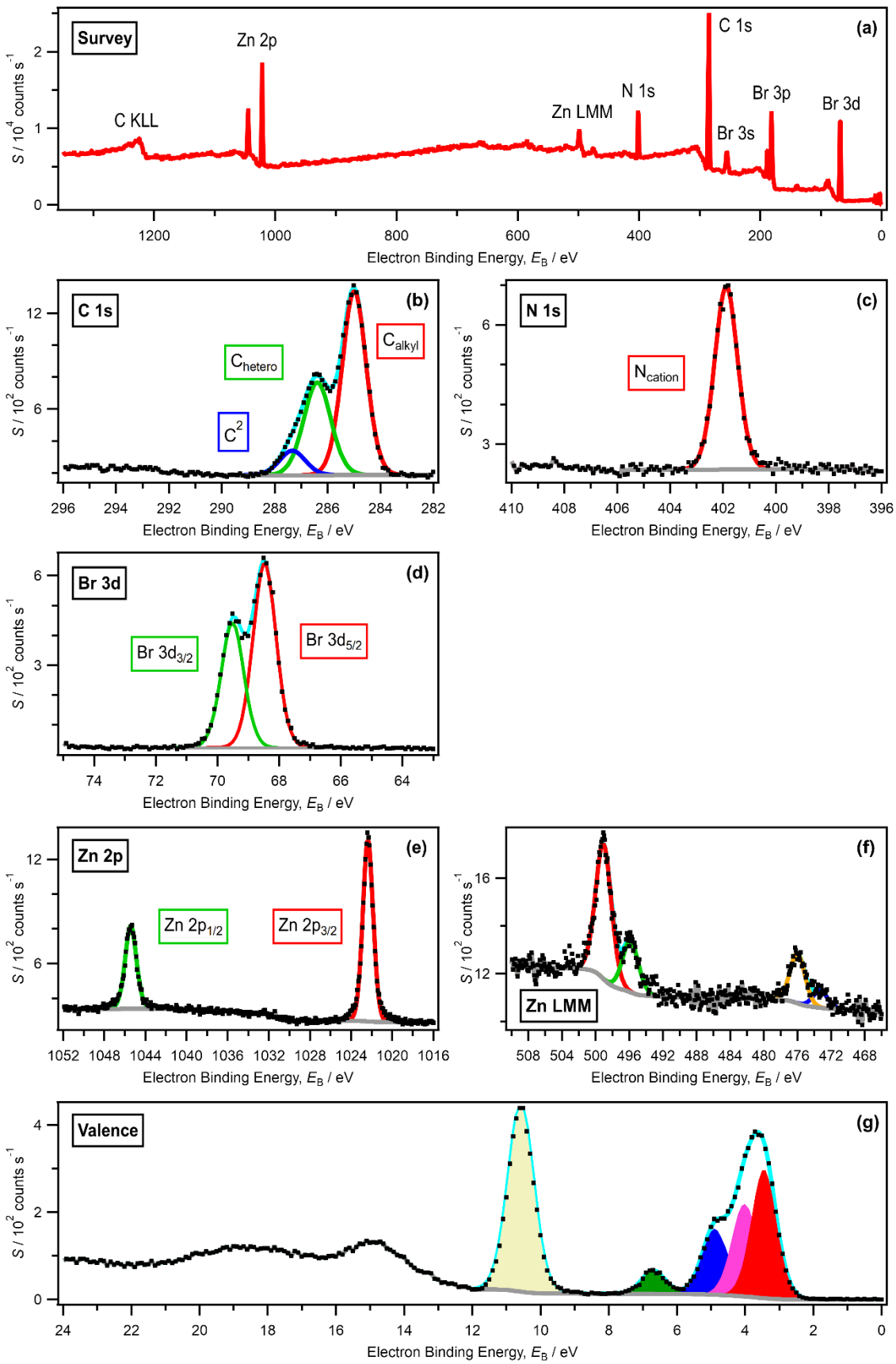


**Figure S9.** (a) Survey, (b-e) core, (f) Auger and (g) valence XP spectra for $[C_8C_1Im]_2[ZnBr_4]$ recorded on laboratory–based XPS apparatus at $h\nu$ = 1486.6 eV. All XP spectra were charge referenced using the method outlined in ESI Section 2.

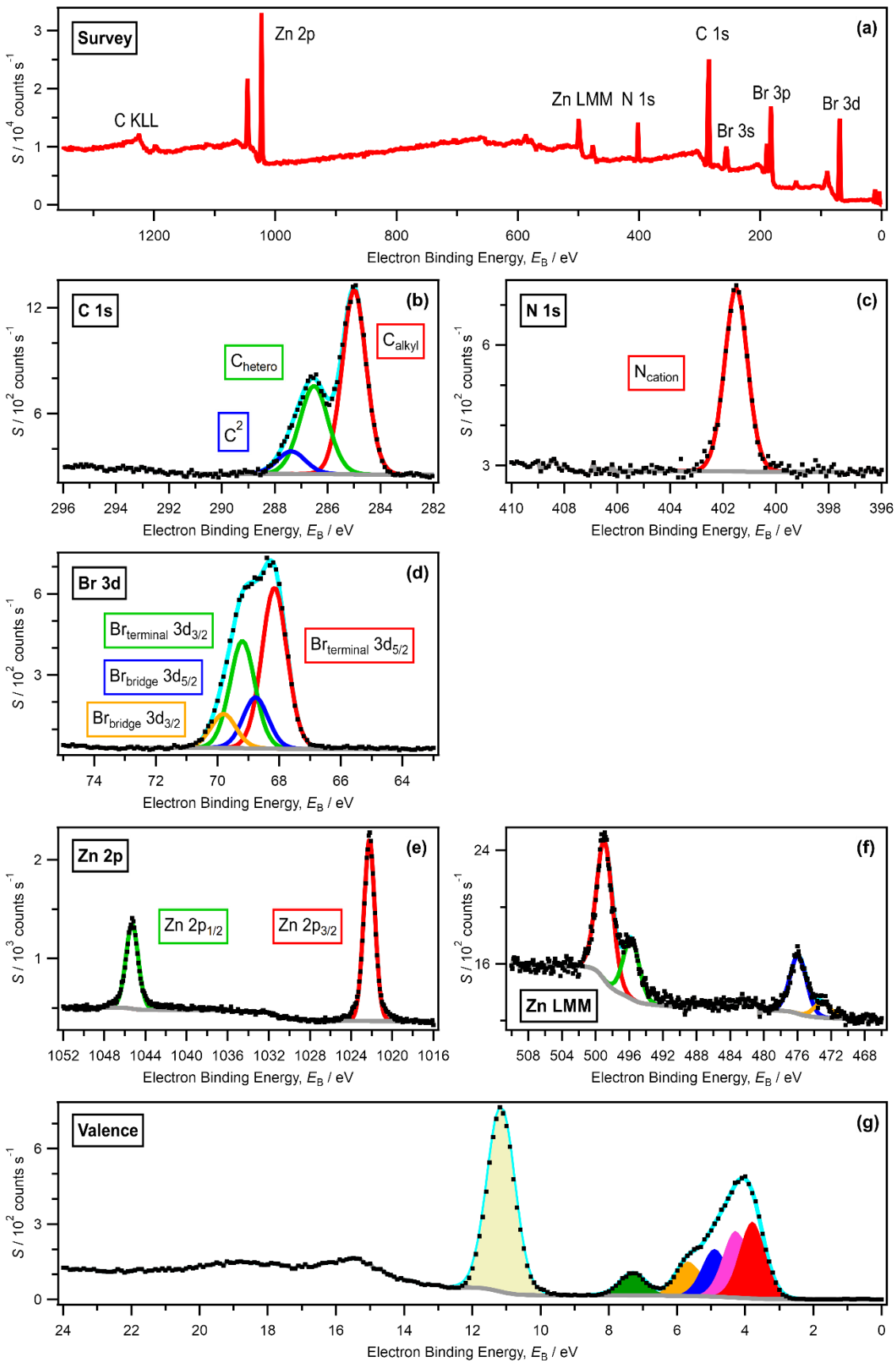


**Figure S10.** (a) Survey, (b-e) core, (f) Auger and (g) valence XP spectra for $[C_8C_1Im]_2[Zn_2Br_6]$ recorded on laboratory–based XPS apparatus at $h\nu$ = 1486.6 eV. All XP spectra were charge referenced using the method outlined in ESI Section 2.

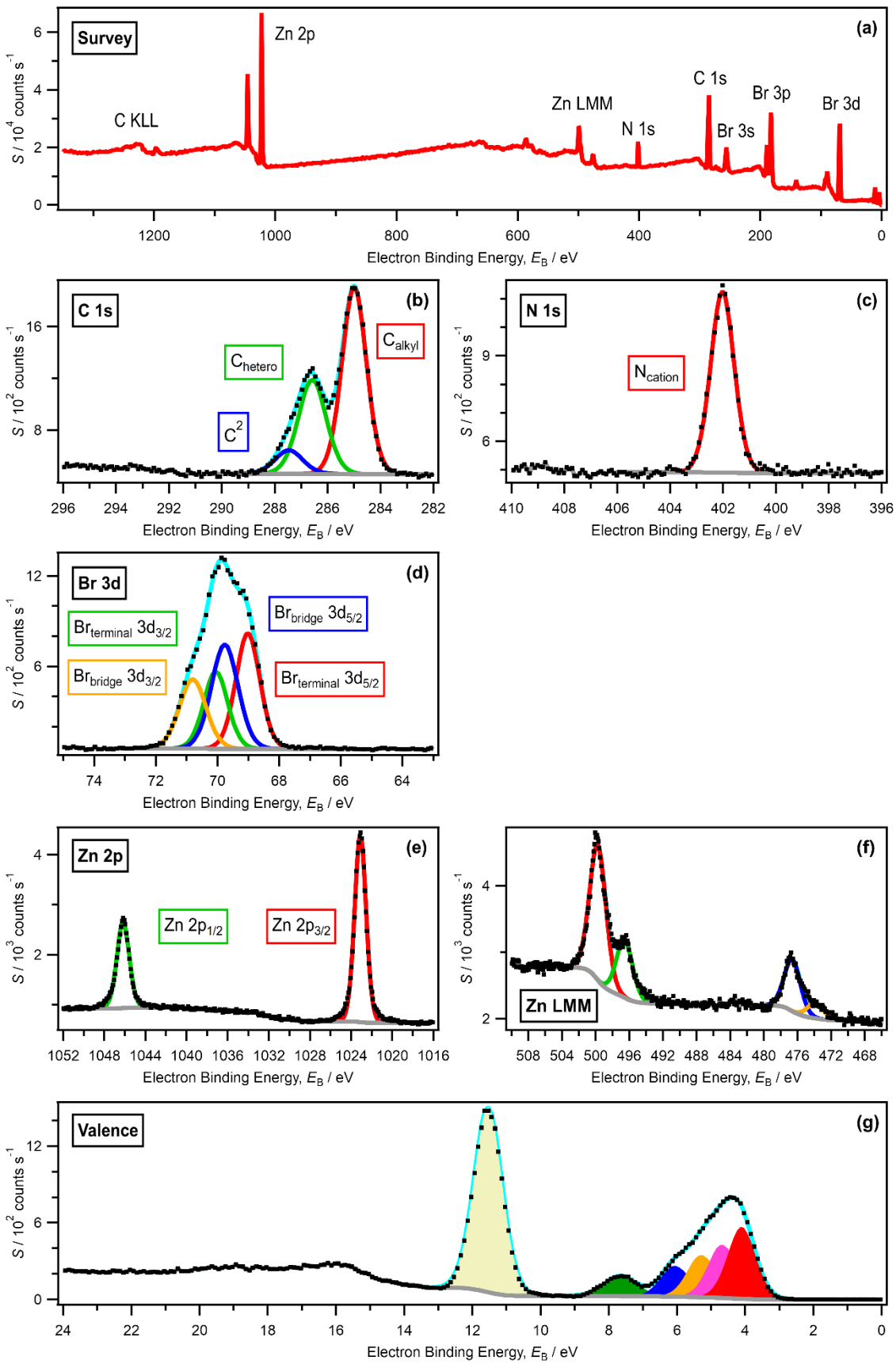


**Figure S11.** (a) Survey, (b-e) core, (f) Auger and (g) valence XP spectra for $[C_8C_1Im]_2[Zn_3Br_8]$ recorded on laboratory–based XPS apparatus at $h\nu$ = 1486.6 eV. All XP spectra were charge referenced using the method outlined in ESI Section 2.

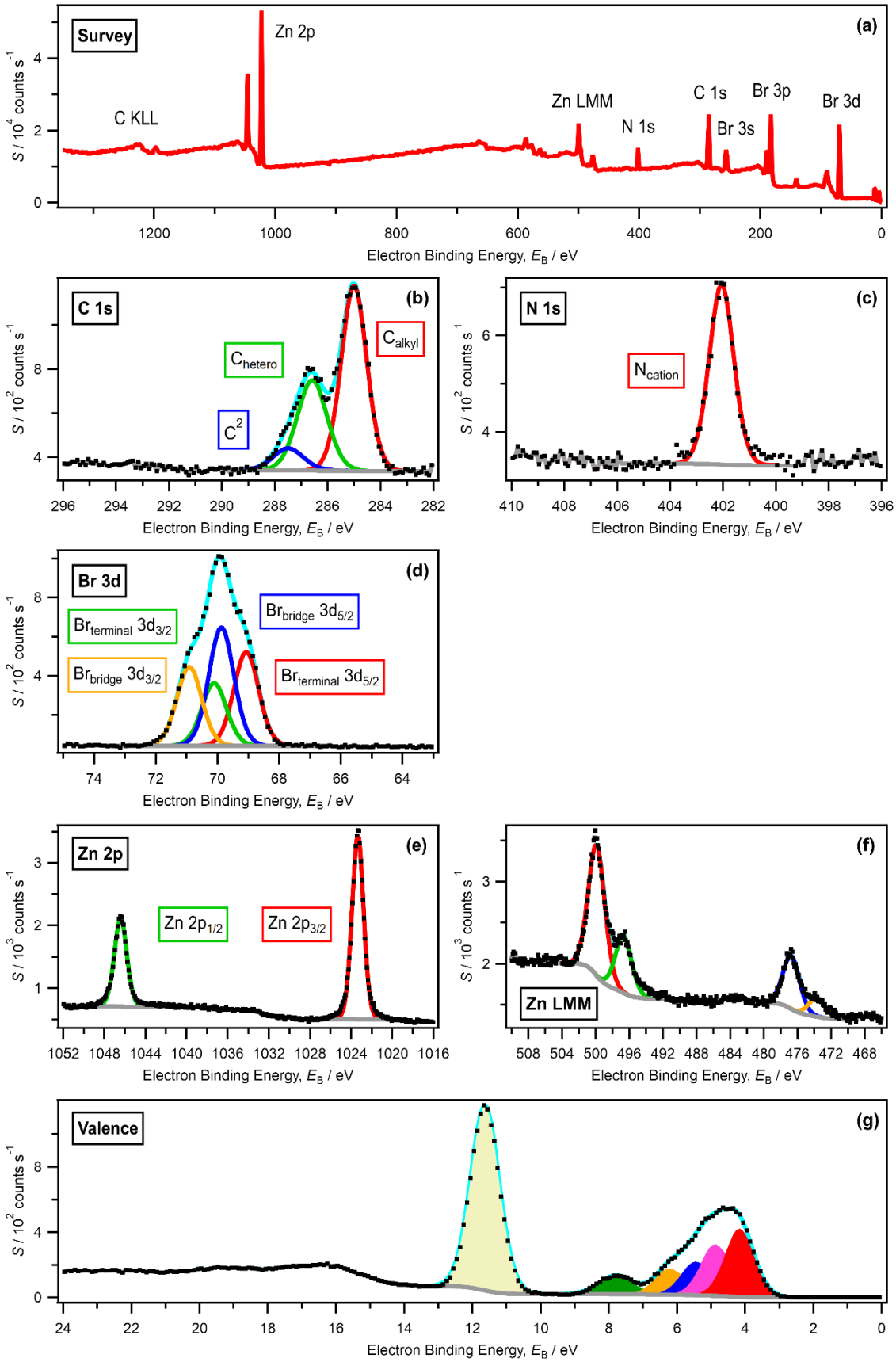


**Figure S12.** (a) Survey, (b-e) core, (f) Auger and (g) valence XP spectra for $[C_8C_1Im]_2[Zn_4Br_{10}]$ recorded on laboratory–based XPS apparatus at $h\nu$ = 1486.6 eV. All XP spectra were charge referenced using the method outlined in ESI Section 2.

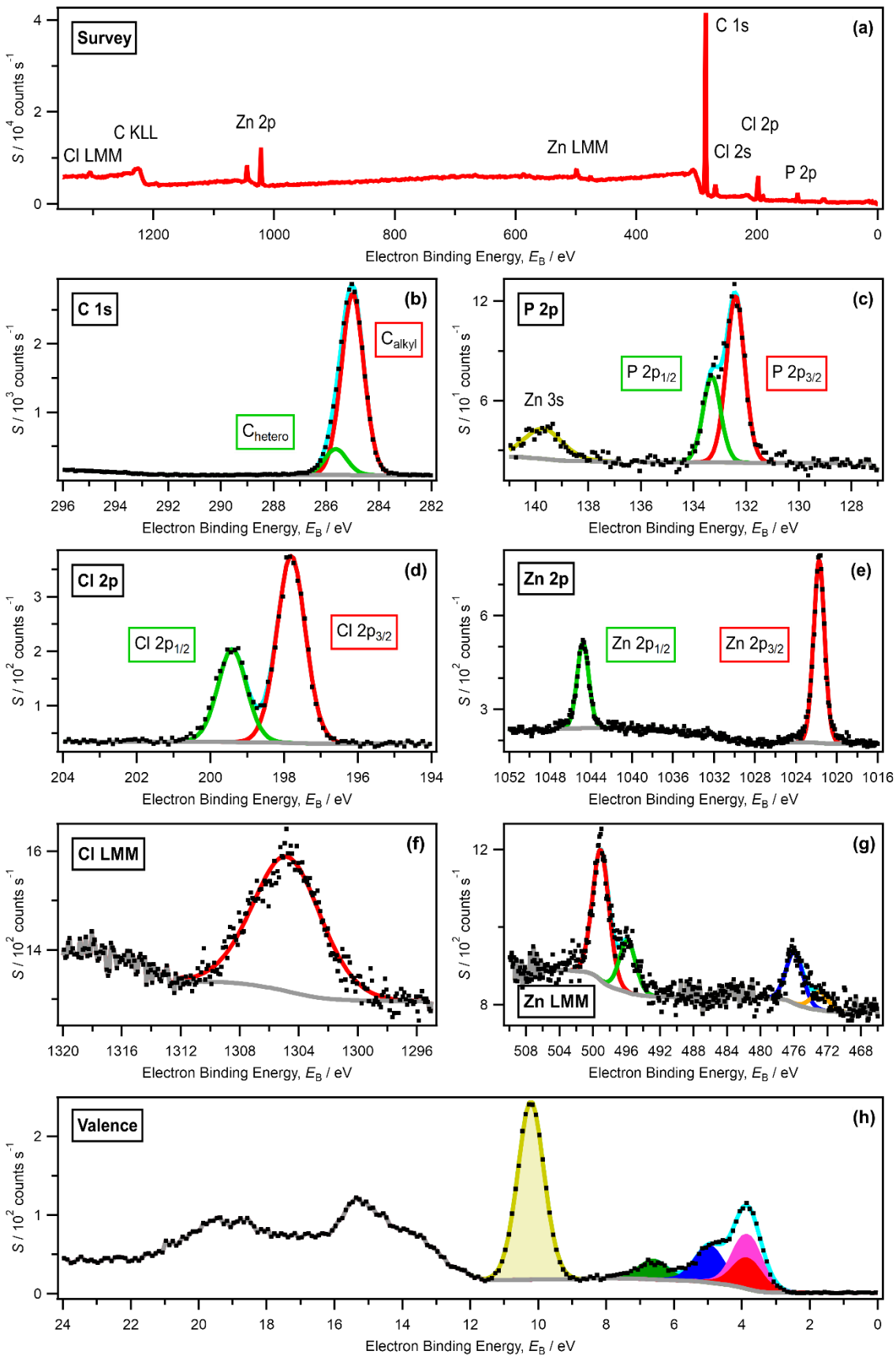


**Figure S13.** (a) Survey, (b-e) core, (f-g) Auger and (h) valence XP spectra for $[P_{6,6,6,14}]_2[ZnCl_4]$ recorded on laboratory–based XPS apparatus at $h\nu$ = 1486.6 eV. All XP spectra were charge referenced using the method outlined in ESI Section 2.

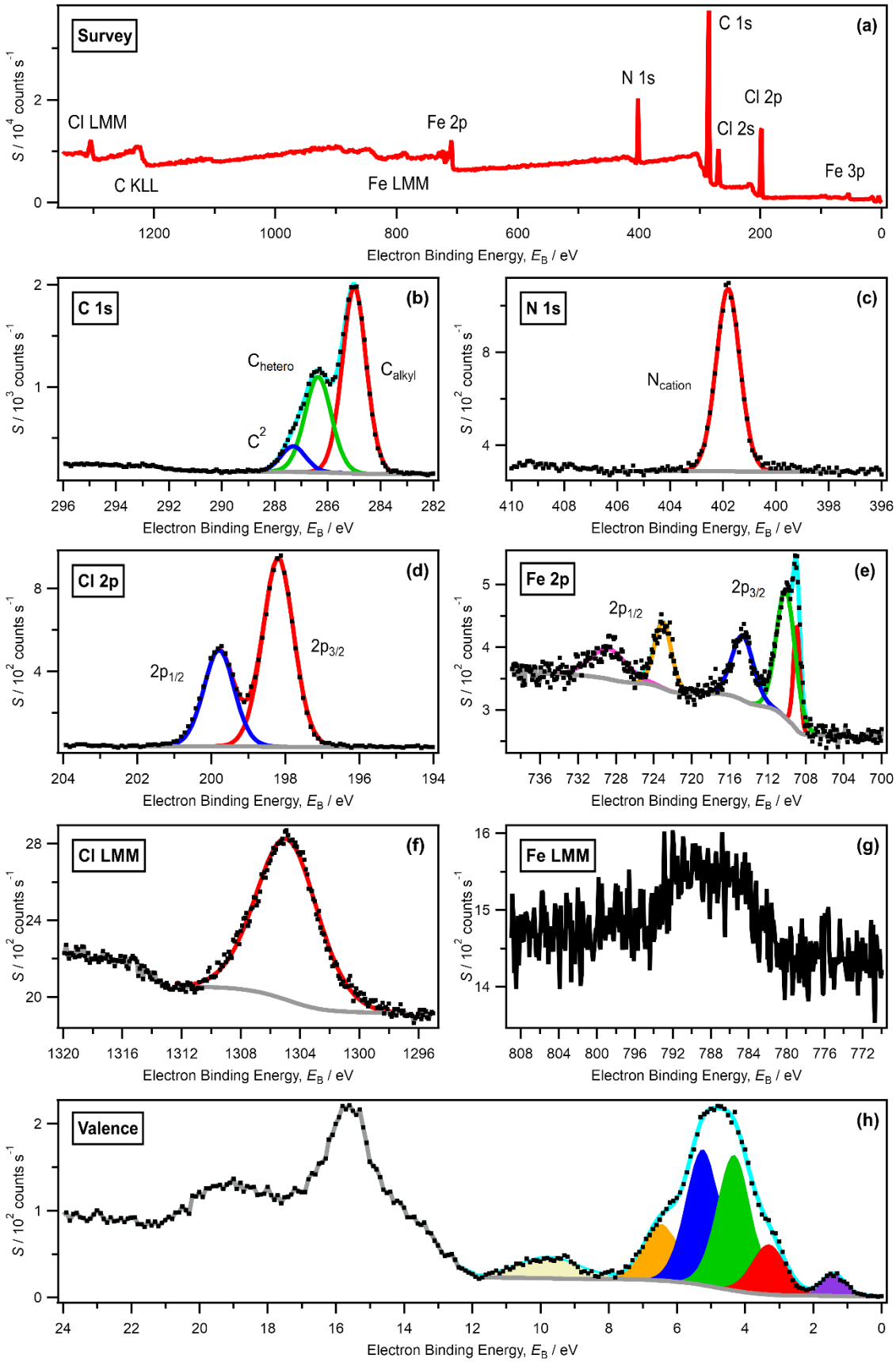


**Figure S14.** (a) Survey, (b-e) core, (f-g) Auger and (h) valence XP spectra for $[C_8C_1Im]_2[FeCl_4]$ recorded on laboratory–based XPS apparatus at $h\nu$ = 1486.6 eV. All XP spectra were charge referenced using the method outlined in ESI Section 2.

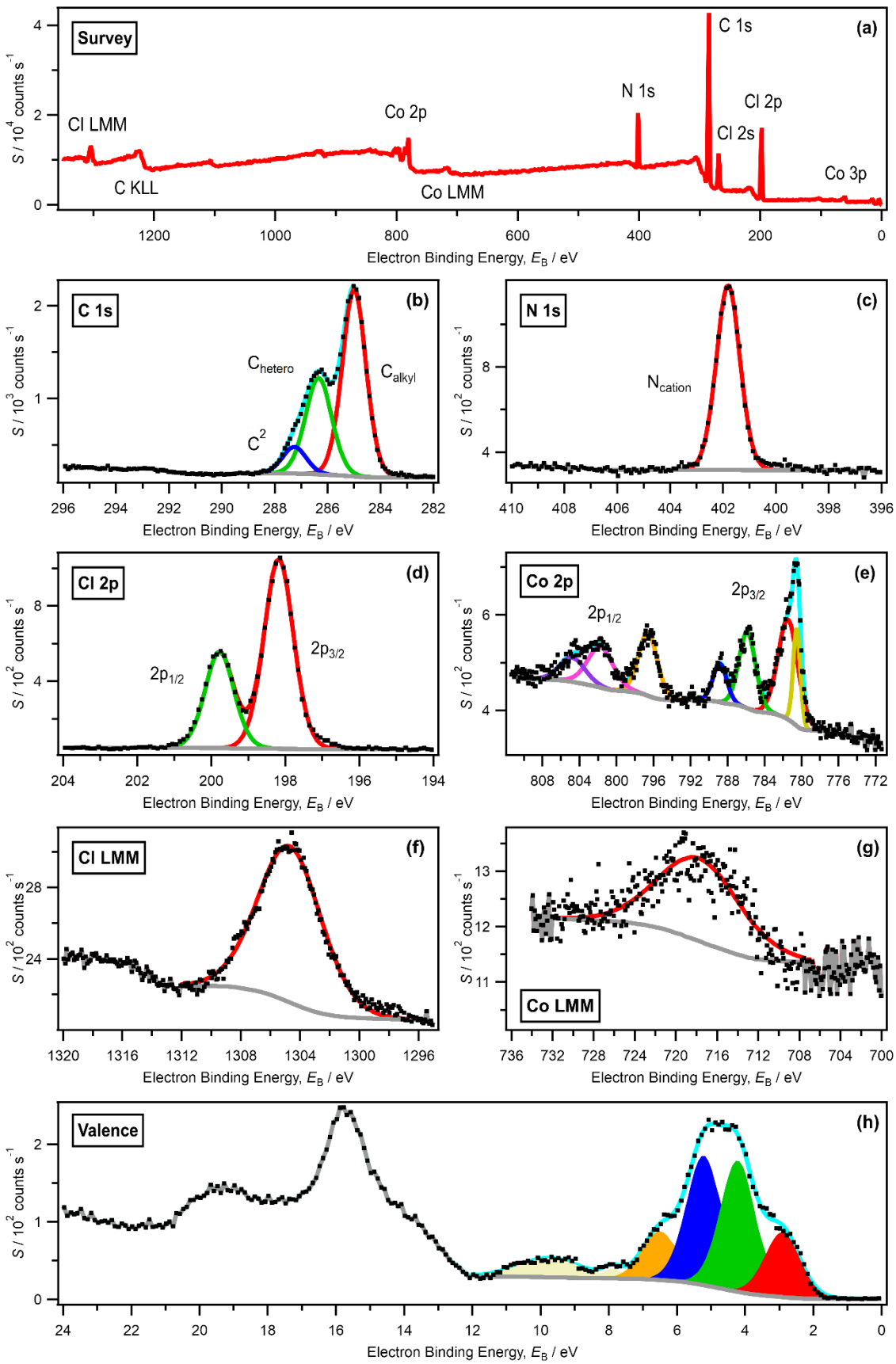


**Figure S15.** (a) Survey, (b-e) core, (f-g) Auger and (h) valence XP spectra for $[C_8C_1Im]_2[CoCl_4]$ recorded on laboratory–based XPS apparatus at $h\nu$ = 1486.6 eV. All XP spectra were charge referenced using the method outlined in ESI Section 2.

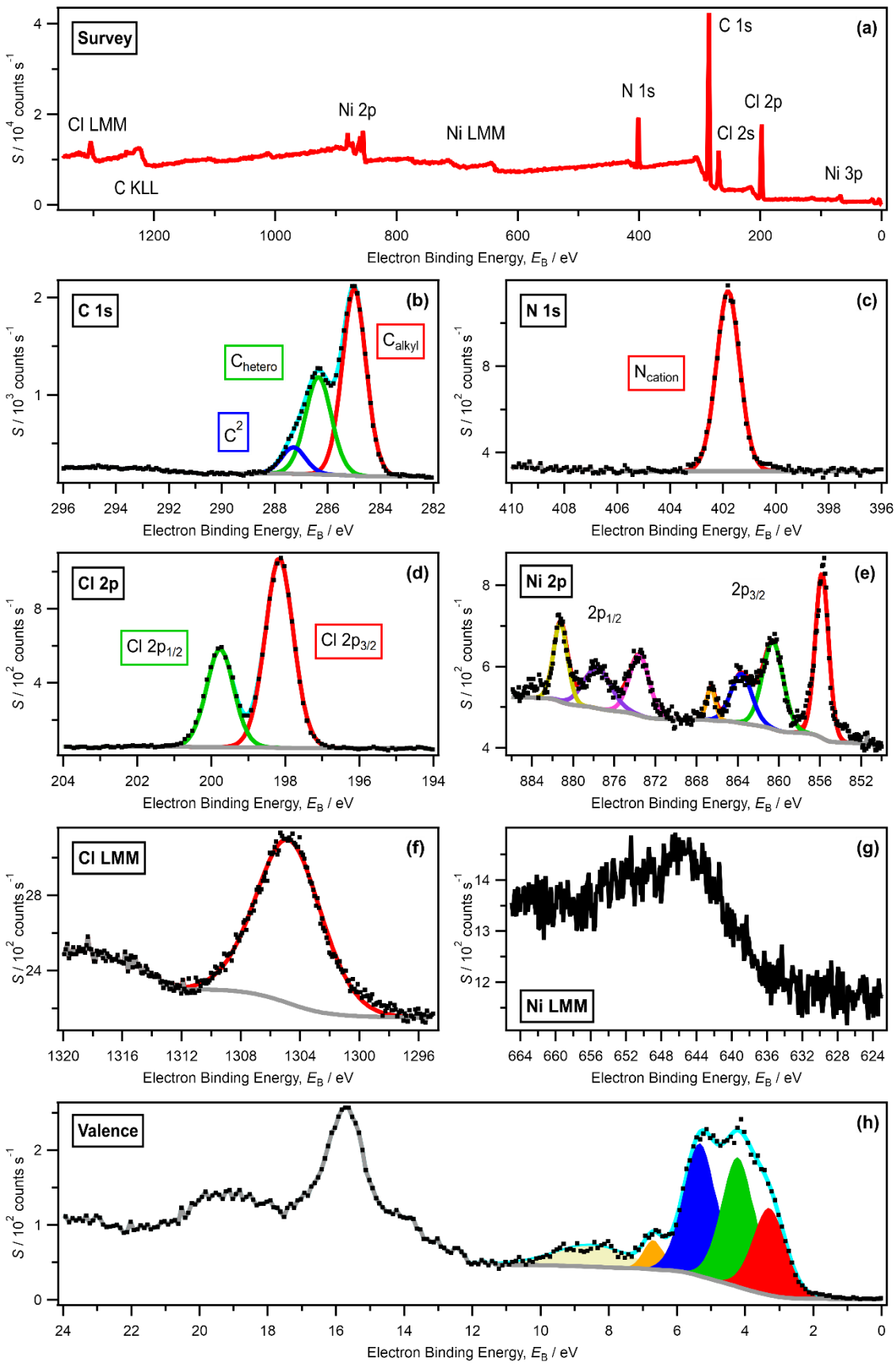


**Figure S16.** (a) Survey, (b-e) core, (f-g) Auger and (h) valence XP spectra for $[C_8C_1Im]_2[NiCl_4]$ recorded on laboratory–based XPS apparatus at $h\nu$ = 1486.6 eV. All XP spectra were charge referenced using the method outlined in ESI Section 2.

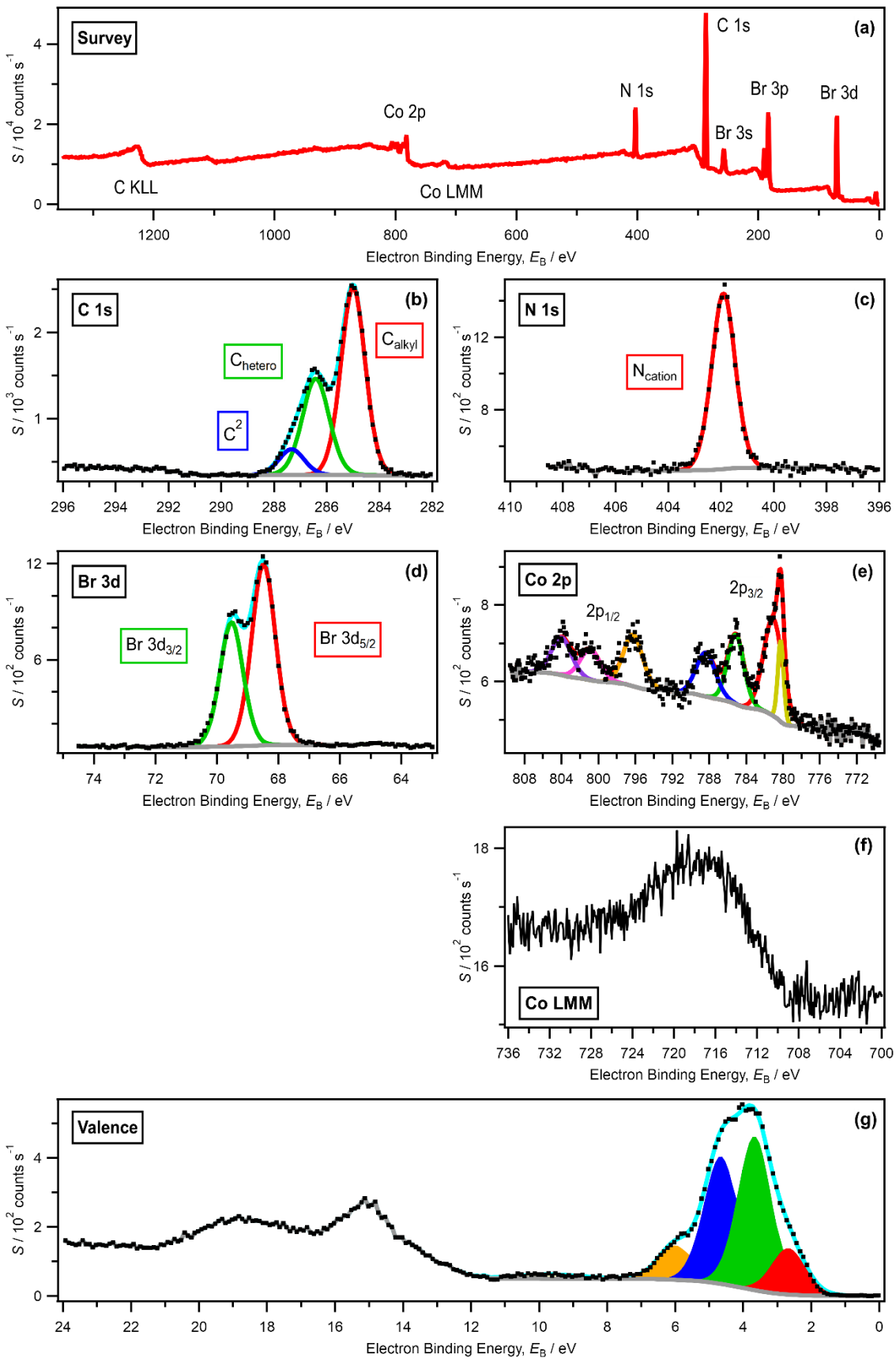


**Figure S17.** (a) Survey, (b-e) core, (f) Auger and (g) valence XP spectra for $[C_8C_1Im]_2[CoBr_4]$ recorded on laboratory–based XPS apparatus at $h\nu$ = 1486.6 eV. All XP spectra were charge referenced using the method outlined in ESI Section 2.

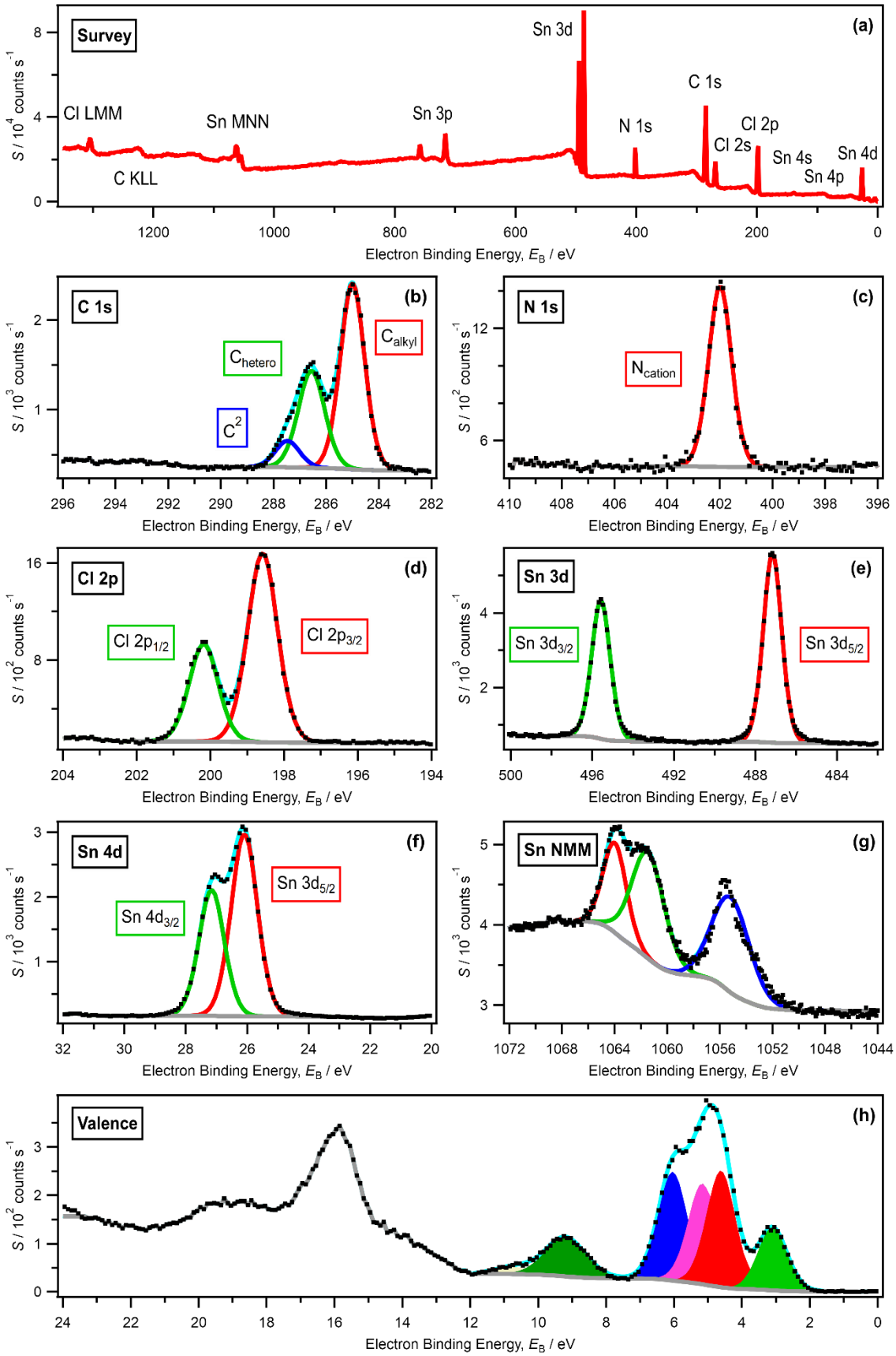


**Figure S18.** (a) Survey, (b-f) core, (g) Auger and (h) valence XP spectra for $[C_8C_1Im][SnCl_3]$ recorded on laboratory–based XPS apparatus at $h\nu$ = 1486.6 eV. All XP spectra were charge referenced using the method outlined in ESI Section 2.

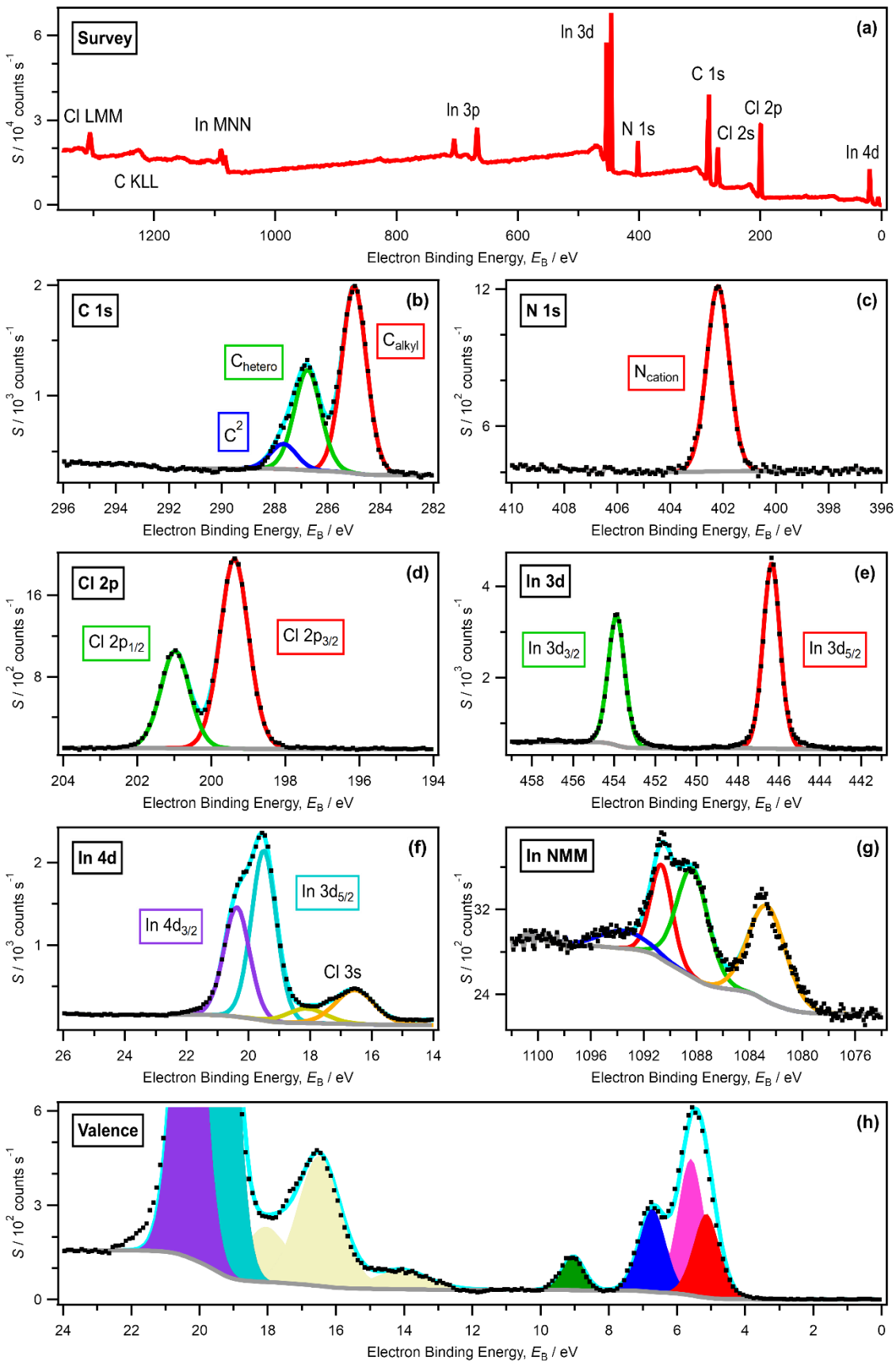


**Figure S19.** (a) Survey, (b-f) core, (g) Auger and (h) valence XP spectra for $[C_8C_1Im][InCl_4]$ recorded on laboratory–based XPS apparatus at $h\nu$ = 1486.6 eV. All XP spectra were charge referenced using the method outlined in ESI Section 2.

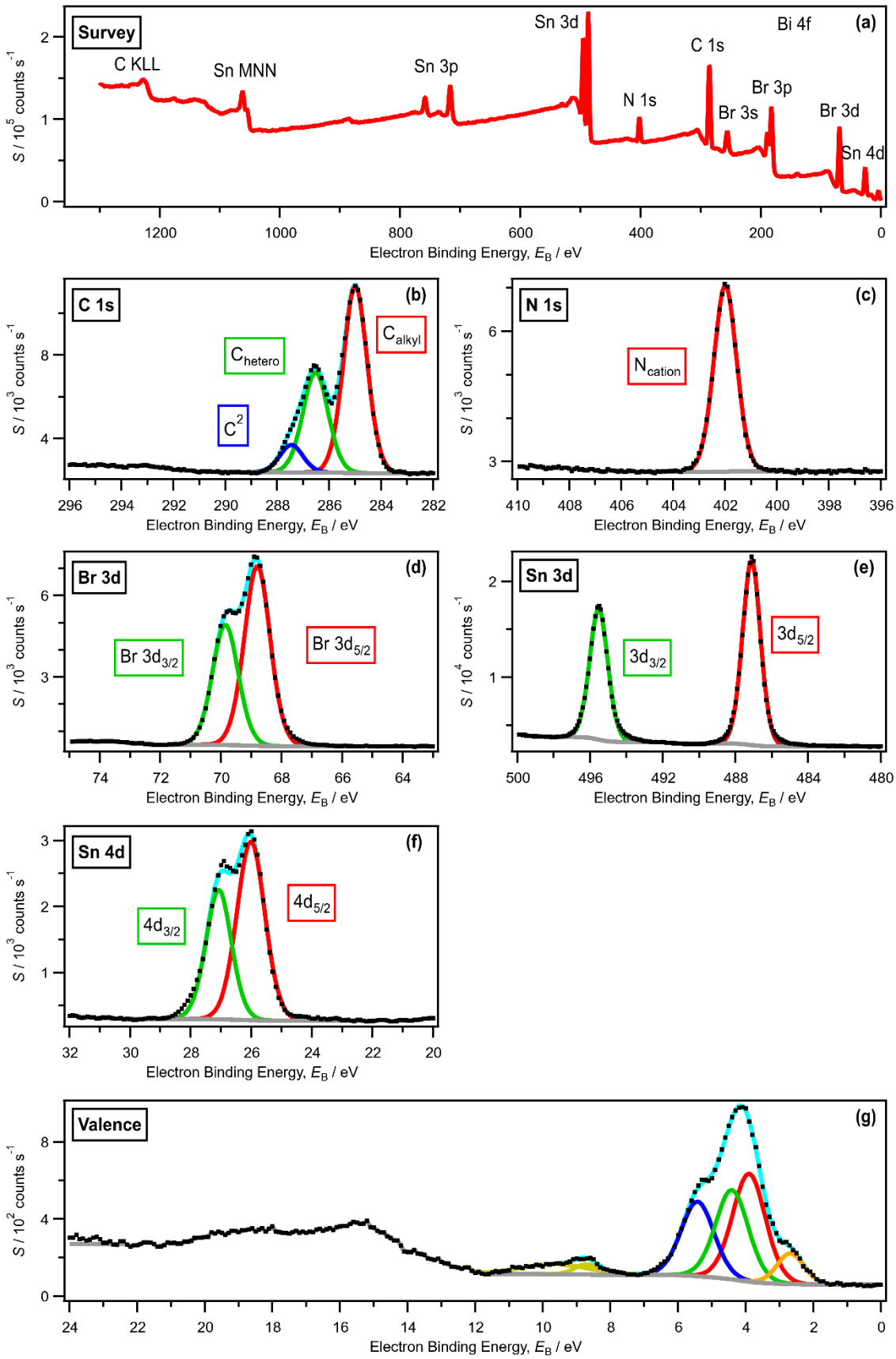


**Figure S20.** (a) Survey, (b-e) core and (f) valence XP spectra for $[C_8C_1Im][SnBr_3]$ recorded on laboratory–based XPS apparatus at $h\nu$ = 1486.6 eV. All XP spectra were charge referenced using the method outlined in ESI Section 2.

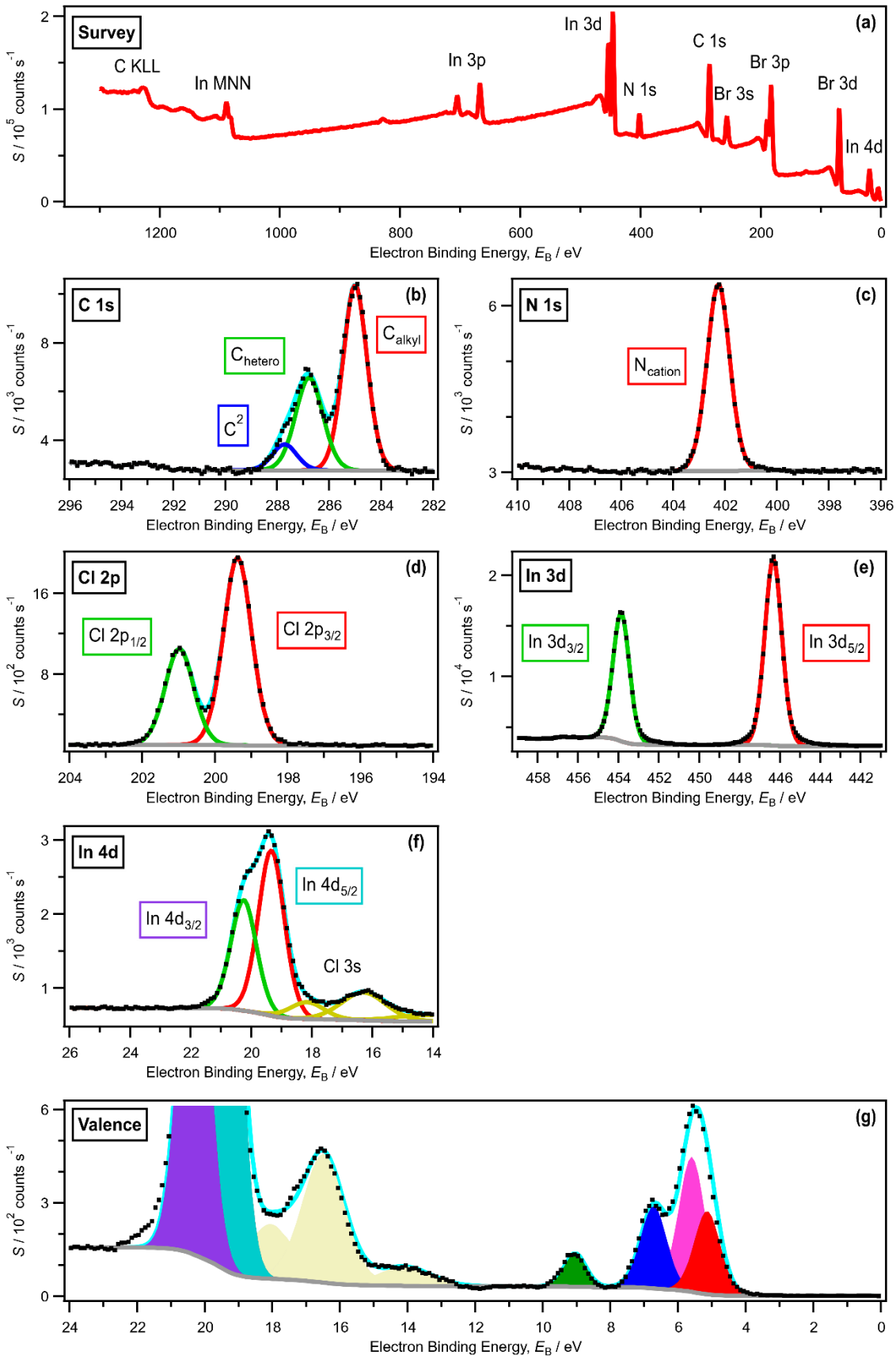


**Figure S21.** (a) Survey, (b-e) core and (f) valence XP spectra for $[C_8C_1Im][InBr_4]$ recorded on laboratory–based XPS apparatus at $h\nu$ = 1486.6 eV. All XP spectra were charge referenced using the method outlined in ESI Section 2.

## 6. Results. XPS: $E_B$(core)

**Table S4.** $E_B$(core) for halozincate-based ILs, $[C_8C_1Im]Cl$ and $[C_8C_1Im]Br$

| | $E_B$ / eV | | | | | | | | | | | | | | | | | |
|---|---|---|---|---|---|---|---|---|---|---|---|---|---|---|---|---|---|---|
| **Sample** | **$C_{alkyl}$ 1s** | **$C_{hetero}$ 1s** | **$C^2$ 1s** | **$N_{cation}$ 1s** | **$Cl_{free}$ $2p_{3/2}$** | **$Cl_{free}$ $2p_{1/2}$** | **$Cl_{terminal}$ $2p_{1/2}$** | **$Cl_{terminal}$ $2p_{1/2}$** | **$Cl_{bridging}$ $2p_{3/2}$** | **$Cl_{bridging}$ $2p_{1/2}$** | **$Br_{free}$ $3d_{5/2}$** | **$Br_{free}$ $3d_{3/2}$** | **$Br_{terminal}$ $3d_{5/2}$** | **$Br_{terminal}$ $3d_{5/2}$** | **$Br_{bridging}$ $3d_{5/2}$** | **$Br_{bridging}$ $3d_{5/2}$** | **Zn $2p_{3/2}$** | **Zn $2p_{1/2}$** |
| $[C_8C_1Im]Cl$ | 285.00 | 286.18 | 287.08 | 401.68 | 196.96 | 198.56 | | | | | | | | | | | | |
| $x$ = 0.33 $[C_8C_1Im]_2$ $[ZnCl_4]$ | 285.00 | 286.36 | 287.30 | 401.82 | | | 198.16 | 199.76 | | | | | | | | | 1022.16 | 1045.23 |
| $x$ = 0.43 $[C_8C_1Im]_4$ $[ZnCl_4]$ $[Zn_2Cl_6]$ | 285.00 | 286.47 | 287.41 | 401.95 | | | 198.48 | 200.08 | 199.25 | 200.85 | | | | | | | 1022.73 | 1045.80 |
| $x$ = 0.50 $[C_8C_1Im]_2$ $[Zn_2Cl_6]$ | 285.00 | 286.53 | 287.49 | 401.97 | | | 198.66 | 200.26 | 199.35 | 200.95 | | | | | | | 1022.90 | 1045.97 |
| $x$ = 0.60 $[C_8C_1Im]_2$ $[Zn_3Cl_8]$ | 285.00 | 286.60 | 287.54 | 402.05 | | | 198.81 | 200.41 | 199.67 | 201.27 | | | | | | | 1023.33 | 1046.40 |
| $x$ = 0.67 $[C_8C_1Im]_2$ $[Zn_4Cl_{10}]$ | 285.00 | 286.60 | 287.55 | 402.06 | | | 198.87 | 200.47 | 199.81 | 201.41 | | | | | | | 1023.41 | 1046.48 |
| $[C_8C_1Im]Br$ | 285.00 | 286.22 | 287.13 | 401.71 | | | | | | | 67.41 | 68.45 | | | | | | |
| $x$ = 0.33 $[C_8C_1Im]_2$ $[ZnBr_4]$ | 285.00 | 286.39 | 287.35 | 401.88 | | | | | | | | | 68.47 | 69.51 | | | 1022.38 | 1045.45 |
| $x$ = 0.50 $[C_8C_1Im]_2$ $[Zn_2Br_6]$ | 285.00 | 286.54 | 287.52 | 401.96 | | | | | | | | | 68.91 | 69.95 | 69.45 | 70.49 | 1022.97 | 1046.04 |
| $x$ = 0.60 $[C_8C_1Im]_2$ $[Zn_3Br_8]$ | 285.00 | 286.59 | 287.48 | 402.03 | | | | | | | | | 69.01 | 70.05 | 69.76 | 70.80 | 1023.11 | 1046.19 |
| $x$ = 0.67 $[C_8C_1Im]_2$ $[Zn_4Br_{10}]$ | 285.00 | 286.60 | 287.52 | 402.06 | | | | | | | | | 69.03 | 70.07 | 69.84 | 70.88 | 1023.37 | 1046.44 |

## 7. Results. XPS: Core

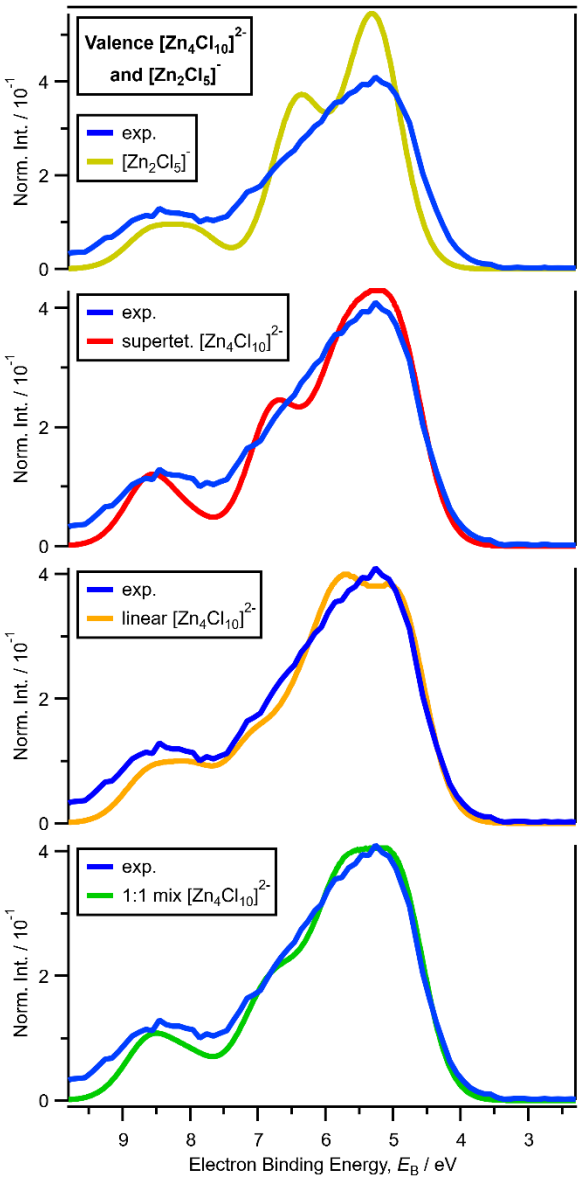


**Figure S22.** Experimental valence XPS for $x$ = 0.67 $[C_8C_1Im]_2[Zn_4Cl_{10}]$ and (1st = top) lone ion SMD calculated valence XPS for supertetrahedron $[Zn_2Cl_5]^-$, (2nd) lone ion SMD calculated valence XPS for supertetrahedron $[Zn_4Cl_{10}]^{2-}$, (3rd) linear $[Zn_4Cl_{10}]^{2-}$, and (4th = bottom) 1:1 mix of supertetrahedron $[Zn_4Cl_{10}]^{2-}$ and linear $[Zn_4Cl_{10}]^{2-}$ (shifted by $E_B$ = -4.67 eV).

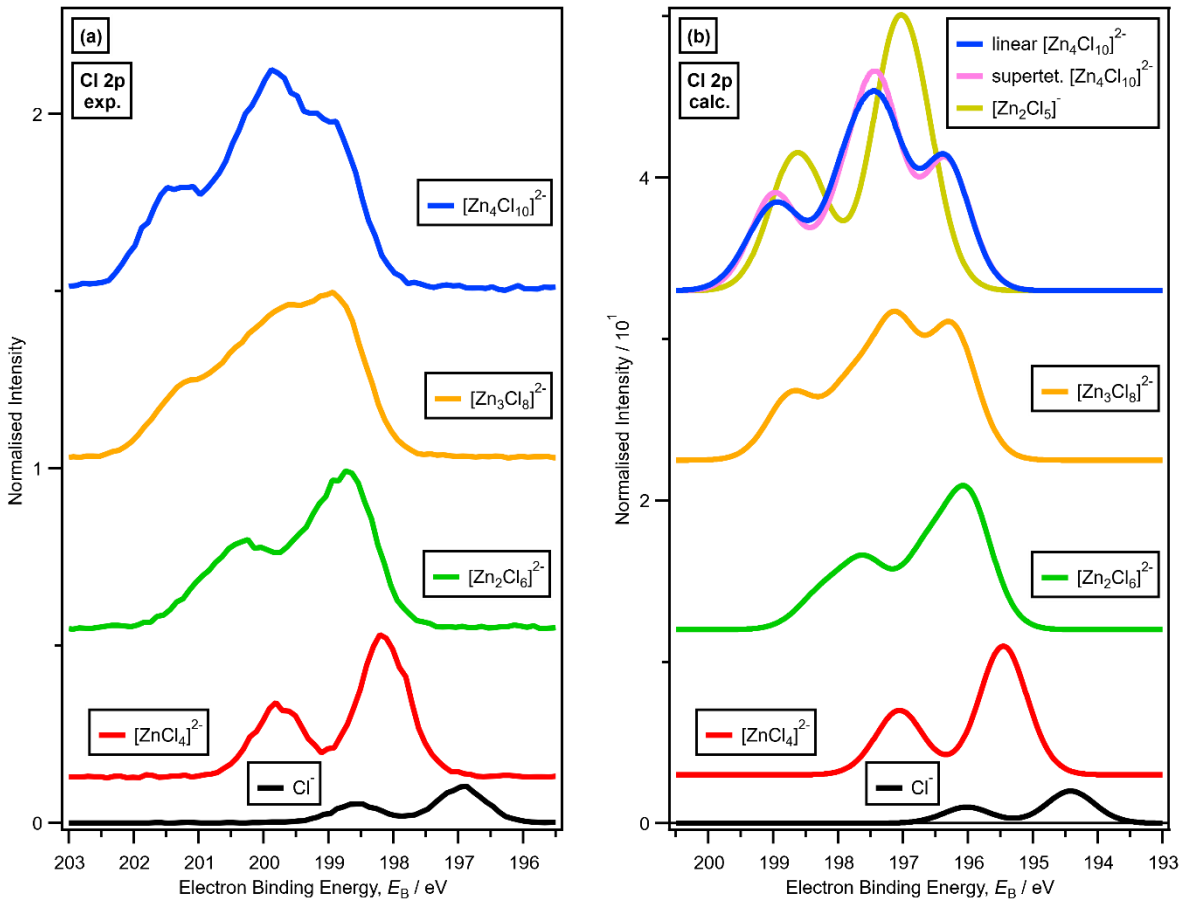


**Figure S23.** (a) Experimental core Cl 2p XPS for $x$ = 0.00 $[C_8C_1Im]Cl$, $x$ = 0.33 $[C_8C_1Im]_2[ZnCl_4]$, $x$ = 0.50 $[C_8C_1Im]_2[Zn_2Cl_6]$, $x$ = 0.60 $[C_8C_1Im]_2[Zn_3Cl_8]$, $x$ = 0.67 $[C_8C_1Im]_2[Zn_4Cl_{10}]$ (vertically offset for clarity). (b) Lone ion SMD calculated core Cl 2p XPS for $Cl^-$, $[ZnCl_4]^{2-}$, $[Zn_2Cl_6]^{2-}$, $[Zn_3Cl_8]^{2-}$, $[Zn_4Cl_{10}]^{2-}$ and $[Zn_2Cl_5]^-$ (vertically offset for clarity).

## 8. Results. XPS: FWHM

FWHM($N_{cation}$ 1s) for $[C_8C_1Im]^+$ were all the same within experimental uncertainty for all *x* (Figure 4b), demonstrating that the FWHM is not dependent on viscosity or any other macroscopic IL property; FWHM are dependent on the molecular cations and anions present in solution.

Given the above findings about only one halozincate species being present at certain *x*, it may appear that there are contradictions in the FWHM data. FWHM(Zn $2p_{3/2}$) was larger for *x* = 0.50 than *x* = 0.33. For both *x* = 0.33 and *x* = 0.50 one anion was present; for *x* = 0.50 $[Zn_2Cl_6]^{2-}$ has two Zn atoms in each anion, and the small variations in the $[Zn_2Cl_6]^{2-}$ structure in the liquid phase give a larger FWHM. This effect is not captured by our approach of calculating a single $[Zn_2Cl_6]^{2-}$ structure; *ab initio* molecular dynamics of $[Zn_2Cl_6]^{2-}$ in an SMD would be helpful here to provide more insight. FWHM(Zn $2p_{3/2}$) was larger for *x* = 0.60 than *x* = 0.50. For *x* = 0.60 where the single anion was $[Zn_3Cl_8]^{2-}$, there are two slightly different types of Zn atom, one Zn atom bound to four bridging Cl, and two Zn atoms bound to two bridging Cl and two terminal Cl. Hence, FWHM(Zn $2p_{3/2}$) was larger for *x* = 0.60 than *x* = 0.50. FWHM(Zn $2p_{3/2}$) was the same within experimental uncertainty for *x* = 0.60 *x* = 0.67. Linear and supertetrahedron $[Zn_4Cl_{10}]^{2-}$ have zinc in two and one electronic environments respectively (from our calculations). The 1:1 ratio of linear and supertetrahedron $[Zn_4Cl_{10}]^{2-}$ gives a similar FWHM to $[Zn_3Cl_8]^{2-}$ which of course has zinc in two different electronic environments.

FWHM(Cl $2p_{3/2}$) (and FWHM(Cl $2p_{1/2}$)) was smaller for *x* = 0.00 and *x* = 0.33 than larger *x* (*i.e*. *x* = 0.50, 0.60, 0.67, ESI Table S5). The same observation can be made for FWHM(Br $3d_{5/2}$) (and FWHM(Br $3d_{3/2}$)), with smaller values for *x* = 0.00 and *x* = 0.33 than larger *x* (ESI Table S5). The greater halide core XPS FWHM values for larger *x* comes from the larger range of electronic environments for larger *x*. There are two origins for this finding. Firstly, for our high symmetry calculated structures for linear $[Zn_4Hal_{10}]^{2-}$, where there are four terminal halides and six bridging halides, the six bridging halides can be placed into two groups (two halides bound only to zinc atoms with only four bridging halides, and four halides bound to one zinc atom with only four bridging halides and one zinc atom with two bridging halides and two terminal halides). These relatively small differences can be observed by comparison of Cl 2p and Br 3d calculated XPS for linear versus supertetrahedron $[Zn_4Hal_{10}]^{2-}$ (Figure 5b and 6b respectively). These differences in the identity of the bridging halides contribute to broadening for linear $[Zn_4Hal_{10}]^{2-}$, but not for any other high symmetry structures. Therefore, the second explanation contributes most to the broadening. For halide core XPS experimental broadening for larger *x* (*i.e*. $[Zn_2Hal_6]^{2-}$, $[Zn_3Hal_8]^{2-}$ and supertetrahedron $[Zn_4Hal_{10}]^{2-}$) is due to nuclear motion in the liquid phase, essentially halozincate anions with lower symmetry than those in our calculations, cause by both vibration of individual Zn-Cl bonds and flexing/rotation/larger motion of more than one Zn-Cl bond.

**Table S5.** FWHM for halozincate-based ILs, $[C_8C_1Im]Cl$ and $[C_8C_1Im]Br$

| | FWHM / eV | | | | | | | | | | | | | | | | | |
|---|---|---|---|---|---|---|---|---|---|---|---|---|---|---|---|---|---|---|
| **Sample** | **$C_{alkyl}$ 1s** | **$C_{hetero}$ 1s** | **$C^2$ 1s** | **$N_{cation}$ 1s** | **$Cl_{free}$ $2p_{3/2}$** | **$Cl_{free}$ $2p_{1/2}$** | **$Cl_{terminal}$ $2p_{1/2}$** | **$Cl_{terminal}$ $2p_{1/2}$** | **$Cl_{bridging}$ $2p_{3/2}$** | **$Cl_{bridging}$ $2p_{1/2}$** | **$Br_{free}$ $3d_{5/2}$** | **$Br_{free}$ $3d_{3/2}$** | **$Br_{terminal}$ $3d_{5/2}$** | **$Br_{terminal}$ $3d_{5/2}$** | **$Br_{bridging}$ $3d_{5/2}$** | **$Br_{bridging}$ $3d_{5/2}$** | **Zn $2p_{3/2}$** | **Zn $2p_{1/2}$** |
| $[C_8C_1Im]Cl$ | 1.05 | 1.21 | 1.01 | 1.03 | 0.90 | 0.87 | | | | | | | | | | | | |
| $x$ = 0.33 $[C_8C_1Im]_2$ $[ZnCl_4]$ | 1.06 | 1.17 | 1.11 | 1.04 | | | 0.91 | 0.90 | | | | | | | | | 1.23 | 1.34 |
| $x$ = 0.43 $[C_8C_1Im]_4$ $[ZnCl_4]$ $[Zn_2Cl_6]$ | 1.09 | 1.18 | 1.10 | 1.07 | | | 0.99 | 0.99 | 0.99 | 0.99 | | | | | | | 1.48 | 1.62 |
| $x$ = 0.50 $[C_8C_1Im]_2$ $[Zn_2Cl_6]$ | 1.09 | 1.19 | 1.14 | 1.02 | | | 0.93 | 0.93 | 0.99 | 0.99 | | | | | | | 1.31 | 1.41 |
| $x$ = 0.60 $[C_8C_1Im]_2$ $[Zn_3Cl_8]$ | 1.11 | 1.17 | 1.12 | 1.08 | | | 0.97 | 0.97 | 1.08 | 1.08 | | | | | | | 1.38 | 1.53 |
| $x$ = 0.67 $[C_8C_1Im]_2$ $[Zn_4Cl_{10}]$ | 1.11 | 1.25 | 1.16 | 1.07 | | | 0.94 | 0.94 | 1.05 | 1.05 | | | | | | | 1.37 | 1.50 |
| $[C_8C_1Im]Br$ | 1.03 | 1.19 | 0.99 | 1.06 | | | | | | | 0.85 | 0.86 | | | | | | |
| $x$ = 0.33 $[C_8C_1Im]_2$ $[ZnBr_4]$ | 1.06 | 1.16 | 1.06 | 1.01 | | | | | | | | | 0.87 | 0.86 | | | 1.18 | 1.31 |
| $x$ = 0.50 $[C_8C_1Im]_2$ $[Zn_2Br_6]$ | 1.08 | 1.22 | 1.22 | 1.01 | | | | | | | | | 0.93 | 0.93 | 1.05 | 1.05 | 1.26 | 1.42 |
| $x$ = 0.60 $[C_8C_1Im]_2$ $[Zn_3Br_8]$ | 1.09 | 1.23 | 1.23 | 1.04 | | | | | | | | | 0.91 | 0.91 | 1.01 | 1.01 | 1.31 | 1.42 |
| $x$ = 0.67 $[C_8C_1Im]_2$ $[Zn_4Br_{10}]$ | 1.10 | 1.26 | 1.32 | 1.08 | | | | | | | | | 0.89 | 0.89 | 0.98 | 0.98 | 1.31 | 1.43 |

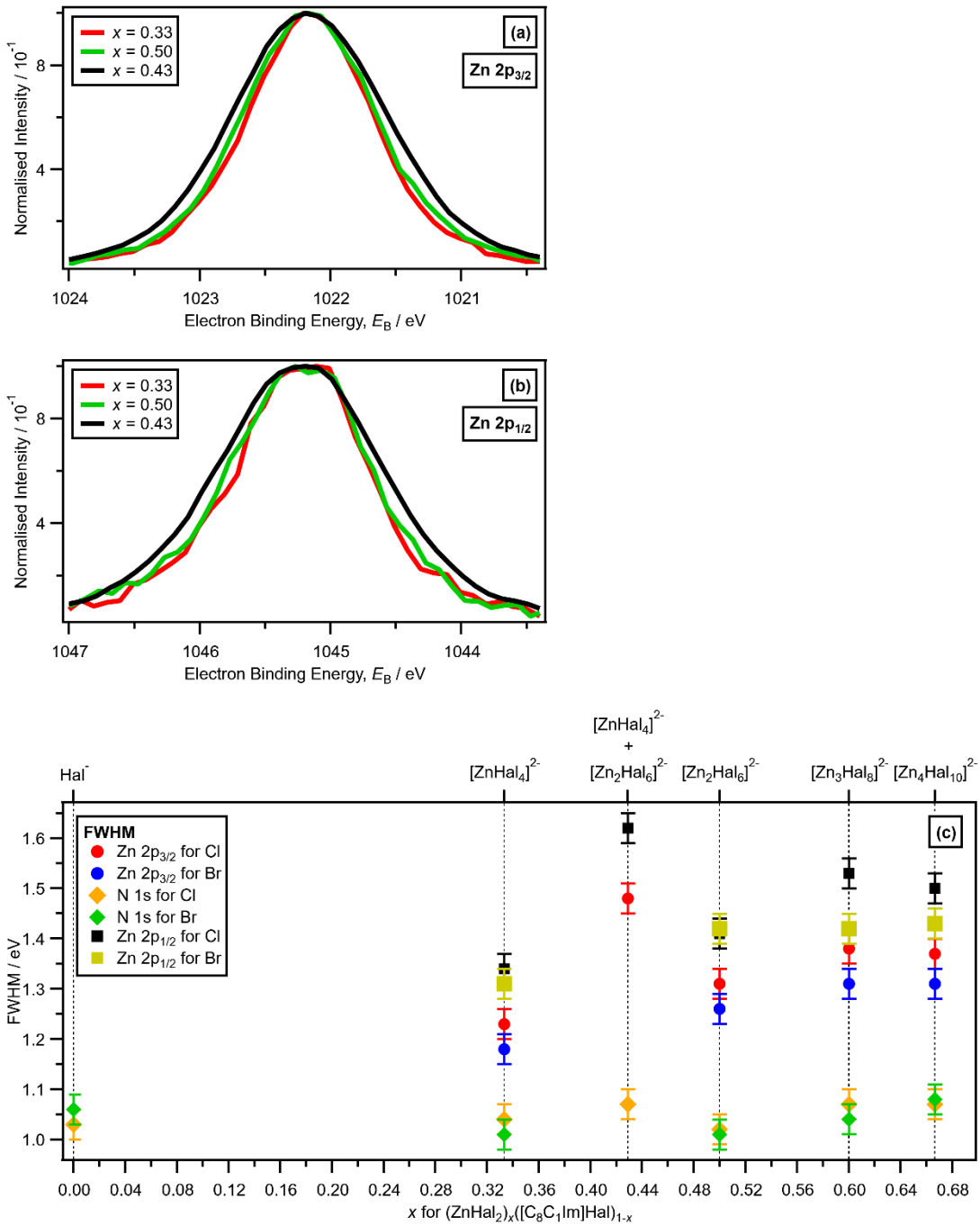


**Figure S24.** (a) Experimental Zn $2p_{3/2}$ XPS for $x$ = 0.33 $[C_8C_1Im]_2[ZnCl_4]$, for $x$ = 0.50 $[C_8C_1Im]_2[Zn_2Cl_6]$, and for $x$ = 0.43 $[C_8C_1Im]_4[ZnCl_4][Zn_2Cl_6]$ (peak intensity normalised to 1, shifted so all $E_B$(Zn $2p_{3/2}$) = 1022.16 eV). (b) Experimental Zn $2p_{1/2}$ XPS for $x$ = 0.33 $[C_8C_1Im]_2[ZnCl_4]$, for $x$ = 0.50 $[C_8C_1Im]_2[Zn_2Cl_6]$, and for $x$ = 0.43 $[C_8C_1Im]_4[ZnCl_4][Zn_2Cl_6]$ (peak intensity normalised to 1, shifted so all $E_B$(Zn $2p_{1/2}$) = 1045.23 eV). (c) Experimental XPS FWHM for Zn $2p_{3/2}$, Zn $2p_{1/2}$, Zn $2p_{3/2}$ and $N_{cation}$ 1s for different $x$ for $([C_8C_1Im]Hal)_{1-x}(ZnHal_2)_x$ from $x$ = 0.00 to $x$ = 0.67.

## 9. Results. XPS: Valence

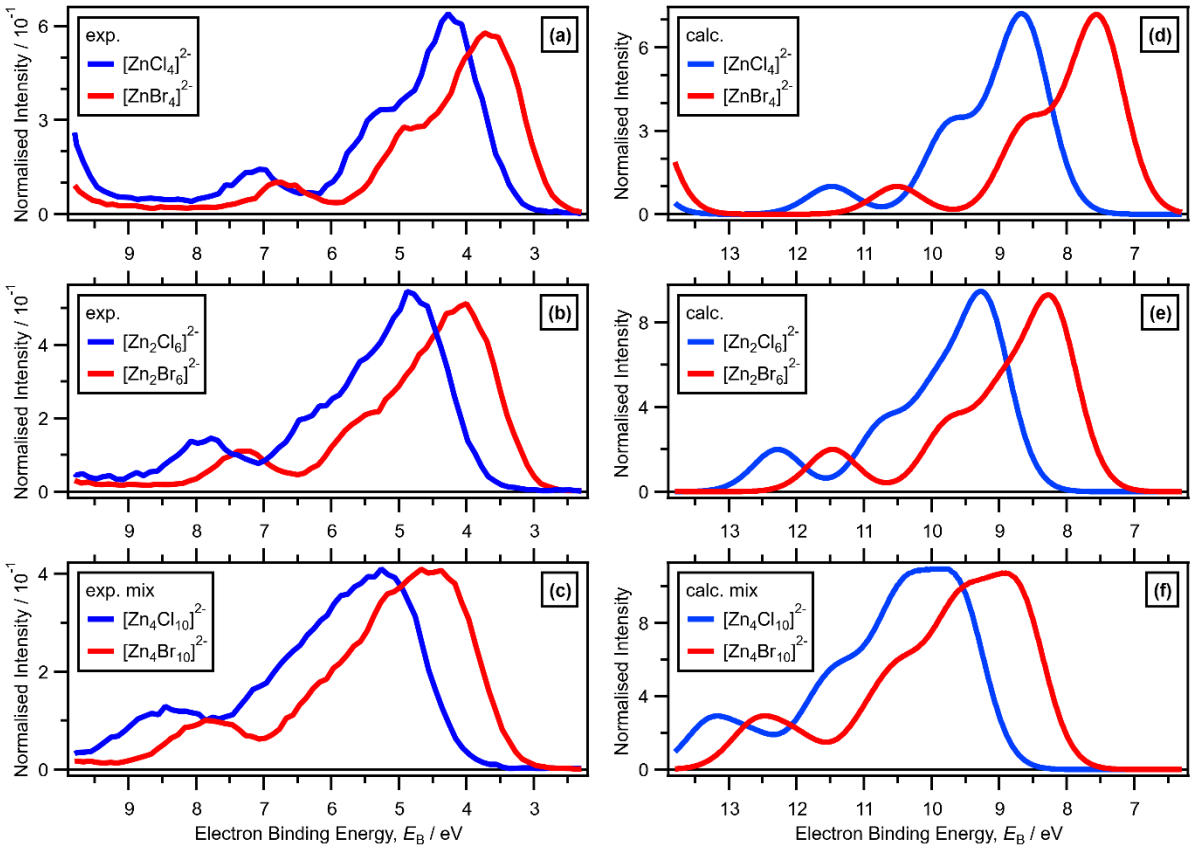


**Figure S25.** Experimental valence XPS for: (a) $x$ = 0.33 $[C_8C_1Im]_2[ZnHal_4]$, (b) $x$ = 0.50 $[C_8C_1Im]_2[Zn_2Hal_6]$, (c) $x$ = 0.67 $[C_8C_1Im]_2[Zn_4Hal_{10}]$. Lone ion SMD calculated valence XPS for: (d) $[ZnHal_4]^{2-}$, (e) $[Zn_2Hal_6]^{2-}$, (f) 1:1 mix of supertetrahedron $[Zn_4Hal_{10}]^{2-}$ and linear $[Zn_4Hal_{10}]^{2-}$ (FWHM = 0.90 eV).

## 10. Results. Calculations: total energies for gas phase calculations

**Table S6.** Experimental and calculated (using gas phase) speciation for chlorozincate and bromozincate anions. The red text in columns 4 and 5 shows calculations that do not agree with the experimental speciation

| $ZnHal_2$ mole fraction, *x* | Reactants | Possible anionic species [a] | $\Delta E$ / kJ mol$^{-1}$ | $\Delta G$ / kJ mol$^{-1}$ |
|---|---|---|---|---|
| | | **2 × $[ZnCl_4]^{2-}$** | | |
| 0.33 | 4 × $Cl^-$ + 2 × $ZnCl_2$ | 2 × $Cl^-$ + 1 × $[Zn_2Cl_6]^{2-}$ | -187.9 | -194.1 |
| | | 2 × $Cl^-$ + 2 × $[ZnCl_3]^-$ | -358.2 | -418.3 |
| | | **2 × $[ZnBr_4]^{2-}$** | | |
| 0.33 | 4 × $Br^-$ + 2 × $ZnBr_2$ | 2 × $Br^-$ + 1 × $[Zn_2Br_6]^{2-}$ | -186.1 | -195.5 |
| | | 2 × $Br^-$ + 2 × $[ZnBr_3]^-$ | -353.5 | -413.5 |
| | | **1 × $[ZnCl_4]^{2-}$ + 1 × $[Zn_2Cl_6]^{2-}$** | | |
| 0.43 | 4 × $Cl^-$ + 3 × $ZnCl_2$ | 1 × $Cl^-$ + 1 × $[ZnCl_3]^-$ + 1 × $[Zn_2Cl_6]^{2-}$ | -179.1 | -209.1 |
| | | 1 × $Cl^-$ + 3 × $[ZnCl_3]^-$ | -349.4 | -433.3 |
| | | **2 × $[Zn_2Cl_6]^{2-}$** | | |
| 0.50 | 4 × $Cl^-$ + 4 × $ZnCl_2$ | 1 × $[ZnCl_4]^{2-}$ + 1 × $[Zn_3Cl_8]^{2-}$ | 57.6 | 49.6 |
| | | 4 × $[ZnCl_3]^-$ | -340.6 | -448.4 |
| | | **2 × $[Zn_2Br_6]^{2-}$** | | |
| 0.50 | 4 × $Br^-$ + 4 × $ZnBr_2$ | 1 × $[ZnBr_4]^{2-}$ + 1 × $[Zn_3Br_8]^{2-}$ | 50.4 | 49.3 |
| | | 4 × $[ZnBr_3]^-$ | -334.9 | -436.0 |
| | | **2 × $[Zn_3Cl_8]^{2-}$** | | |
| | | 1 × $[Zn_2Cl_6]^{2-}$ + 1 × linear $[Zn_4Cl_{10}]^{2-}$ | 30.1 | 29.9 |
| 0.60 | 4 × $Cl^-$ + 6 × $ZnCl_2$ | 1 × $[Zn_2Cl_6]^{2-}$ + 1 × supertetrahedron $[Zn_4Cl_{10}]^{2-}$ | 7.4 | 22.4 |
| | | 2 × $[ZnCl_3]^-$ + 1 × supertetrahedron $[Zn_4Cl_{10}]^{2-}$ | -160.1 | -195.6 |
| | | 2 × $[ZnCl_3]^-$ + 1 × linear $[Zn_4Cl_{10}]^{2-}$ | -137.3 | -188.1 |
| | | **2 × $[Zn_3Br_8]^{2-}$** | | |
| 0.60 | 4 × $Br^-$ + 6 × $ZnBr_2$ | 1 × $[Zn_2Br_6]^{2-}$ + 1 × linear $[Zn_4Br_{10}]^{2-}$ | 30.1 | 29.9 |
| | | 1 × $[Zn_2Br_6]^{2-}$ + 1 × supertetrahedron $[Zn_4Br_{10}]^{2-}$ | 7.4 | 22.4 |
| | | **1 × linear $[Zn_4Cl_{10}]^{2-}$** | | |
| 0.67 | 2 × $Cl^-$ + 4 × $ZnCl_2$ | **1 × supertetrahedron $[Zn_4Cl_{10}]^{2-}$** | -28.87 | -19.0 |
| | | **2 × $[Zn_2Cl_5]^-$** | -82.3 | -128.3 |
| | | **1 × linear $[Zn_4Br_{10}]^{2-}$** | | |
| 0.67 | 2 × $Br^-$ + 4 × $ZnBr_2$ | **1 × supertetrahedron $[Zn_4Br_{10}]^{2-}$** | -22.76 | -7.6 |

[a] Experimental speciation given in bold in this column

## 11. Results. XPS: halometallates with one halide electronic environment

As well as the halozincates, a large number of other halometallate-forming ILs gave one macroscopic halide electronic environment and therefore one halometallate anion: $x$ = 0.33 gave $[MHal_4]^{2-}$ for M = $Zn^{2+}$, $Ni^{2+}$, $Co^{2+}$, $Fe^{2+}$ and Hal = Cl, Br (Figure 2 and ESI Figure S26 and ESI Figure S27); $x$ = 0.50 gave $[InHal_4]^-$ for Hal = Cl and Br (ESI Figure S26 and ESI Figure S27); $x$ = 0.50 gave $[SnHal_3]^-$ for Hal = Cl and Br (ESI Figure S26 and ESI Figure S27). Halometallate anions such as $[CoCl_4]^{2-}$ have been known to be $T_d$ since the 1960s.[5] Our results point to these four coordinate halometallate anions all forming $T_d$ symmetry, with relatively little contribution from M-Hal bond vibration; $[SnHal_3]^-$ gives $C_{3v}$ symmetry (which can be thought of as a distorted tetrahedral) given the stereochemically active lone pair.[6]

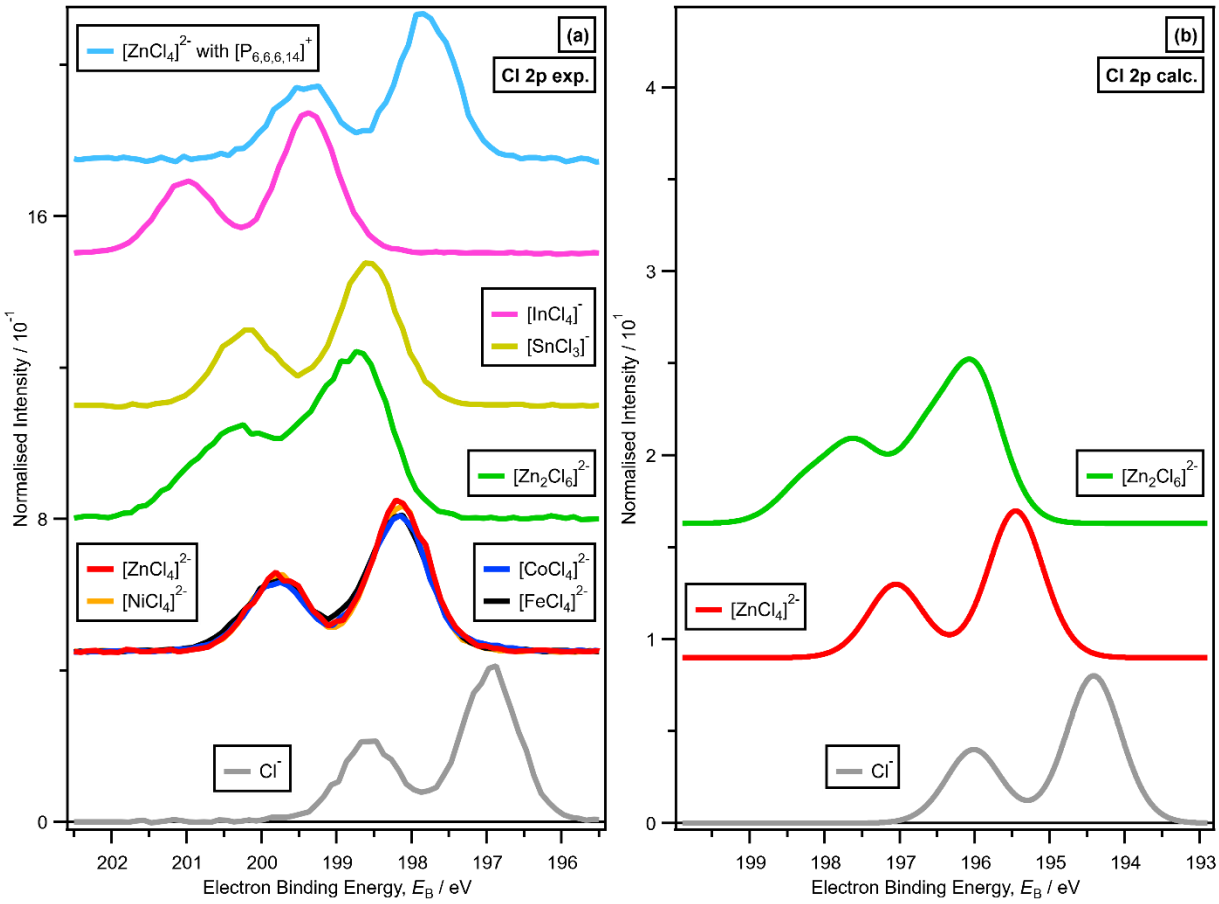


**Figure S26.** (a) Experimental core Cl 2p XPS for $x$ = 0.00 $[C_8C_1Im]Cl$, $x$ = 0.33 $[C_8C_1Im]_2[ZnCl_4]$, $x$ = 0.33 $[C_8C_1Im]_2[NiCl_4]$, $x$ = 0.33 $[C_8C_1Im]_2[CoCl_4]$, $x$ = 0.33 $[C_8C_1Im]_2[FeCl_4]$, $x$ = 0.50 $[C_8C_1Im]_2[Zn_2Cl_6]$, $x$ = 0.50 $[C_8C_1Im][SnCl_3]$, $x$ = 0.50 $[C_8C_1Im][InCl_4]$, (vertically offset for clarity). (b) Lone ion SMD calculated core Cl 2p XPS for $Cl^-$, $[ZnCl_4]^{2-}$, $[Zn_2Cl_6]^{2-}$ (vertically offset for clarity).

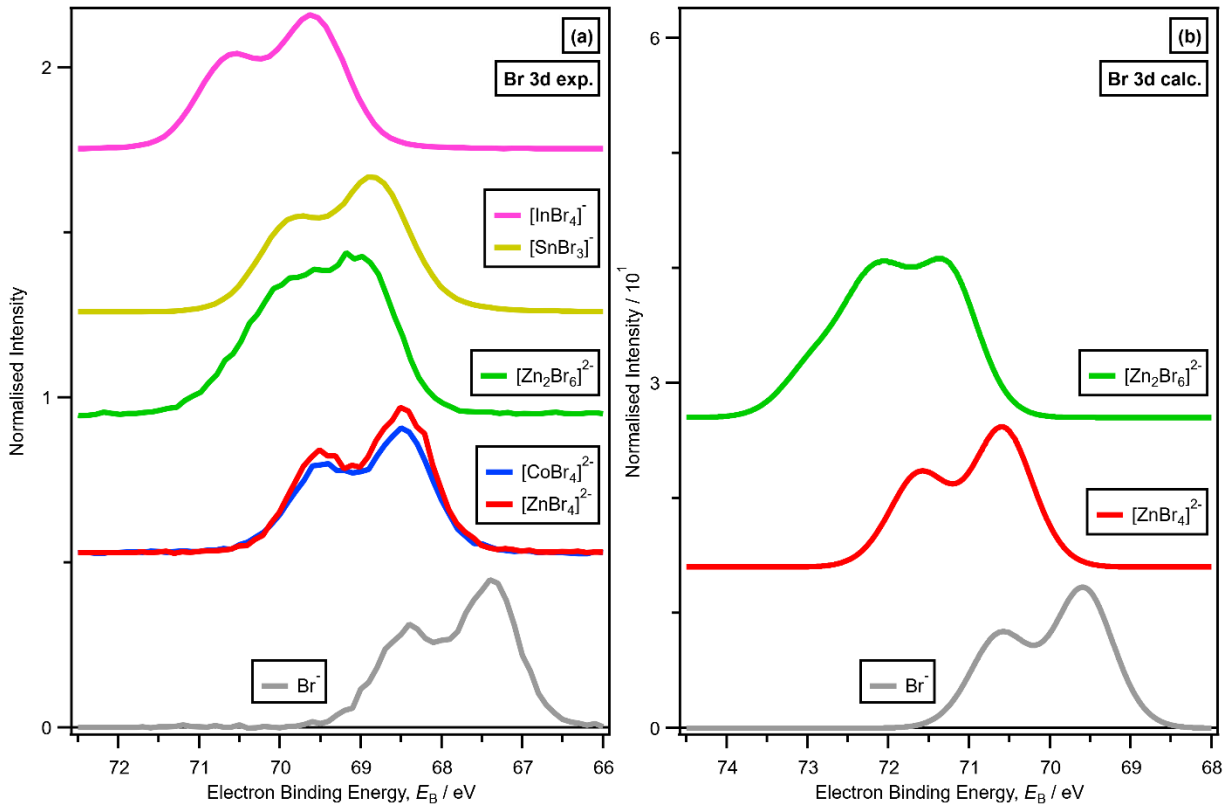


**Figure S27.** (a) Experimental core Br 3d XPS for $x$ = 0.00 $[C_8C_1Im]Br$, $x$ = 0.33 $[C_8C_1Im]_2[ZnBr_4]$, $x$ = 0.33 $[C_8C_1Im]_2[CoBr_4]$, $x$ = 0.50 $[C_8C_1Im]_2[Zn_2Br_6]$, $x$ = 0.50 $[C_8C_1Im][SnBr_3]$, $x$ = 0.50 $[C_8C_1Im][InBr_4]$, (vertically offset for clarity). (b) Lone ion SMD calculated core Br 3d XPS for $Br^-$, $[ZnBr_4]^{2-}$, $[Zn_2Br_6]^{2-}$ (vertically offset for clarity).

## 12. Results. Effect of basis set on calculated Cl 2p XPS

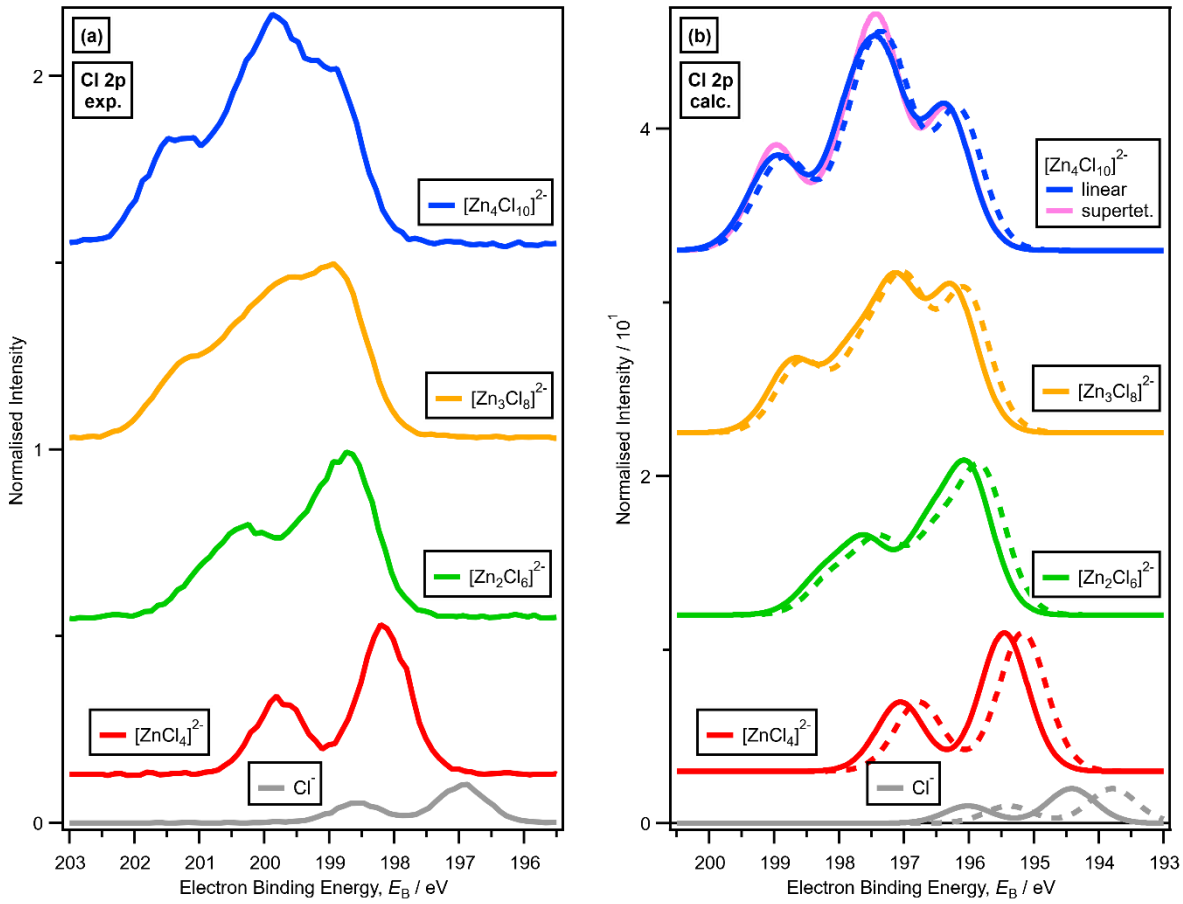


**Figure S28.** (a) Experimental core Cl 2p XPS for $x$ = 0.00 $[C_8C_1Im]Cl$, $x$ = 0.33 $[C_8C_1Im]_2[ZnCl_4]$, $x$ = 0.50 $[C_8C_1Im]_2[Zn_2Cl_6]$, $x$ = 0.60 $[C_8C_1Im]_2[Zn_3Cl_8]$, $x$ = 0.67 $[C_8C_1Im]_2[Zn_4Cl_{10}]$ (vertically offset for clarity). (b) Lone ion SMD calculated core Cl 2p XPS for $Cl^-$, $[ZnCl_4]^{2-}$, $[Zn_2Cl_6]^{2-}$, $[Zn_3Cl_8]^{2-}$ and $[Zn_4Cl_{10}]^{2-}$ (vertically offset for clarity) for different basis sets: QZVPP (solid lines) and TZVPP (dashed lines).

## 13. Results. Effect of solvation environment on calculated Cl 2p XPS

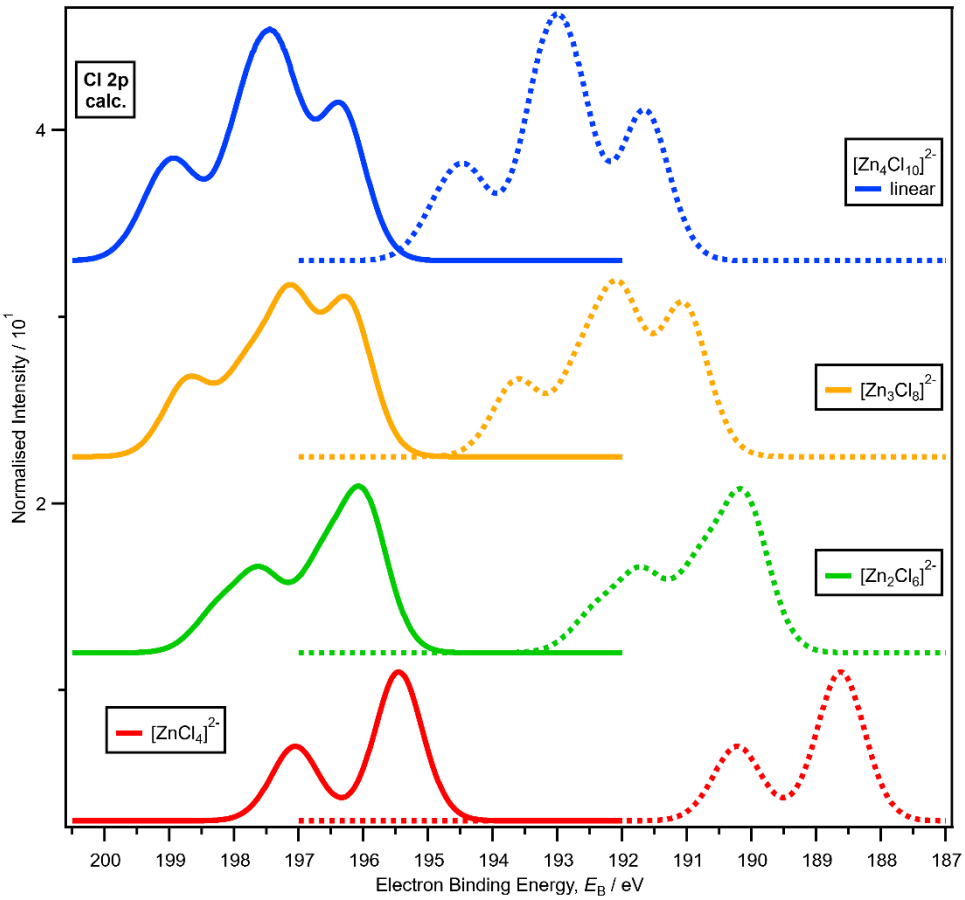


**Figure S29.** Lone ion SMD (solid lines) and gas phase (dashed lines) calculated core Cl 2p XPS for $[ZnCl_4]^{2-}$, $[Zn_2Cl_6]^{2-}$, $[Zn_3Cl_8]^{2-}$ and $[Zn_4Cl_{10}]^{2-}$ (vertically offset for clarity), all with the QZVPP basis set.

## 14. References


1. J. M. Seymour, E. Gousseva, A. I. Large, C. J. Clarke, P. Licence, R. M. Fogarty, D. A. Duncan, P. Ferrer, F. Venturini, R. A. Bennett, R. G. Palgrave and K. R. J. Lovelock, *Phys. Chem. Chem. Phys.*, 2021, **23**, 20957-20973.
2. E. Gousseva, F. K. Towers Tompkins, J. M. Seymour, L. G. Parker, C. J. Clarke, R. G. Palgrave, R. A. Bennett, R. Grau-Crespo and K. R. J. Lovelock, 2024, submitted.
3. C. J. Clarke, H. Baaqel, R. P. Matthews, Y. Y. Chen, K. R. J. Lovelock, J. P. Hallett and P. Licence, *Green Chem.*, 2022, **24**, 5800-5812.
4. R. M. Fogarty, R. G. Palgrave, R. A. Bourne, K. Handrup, I. J. Villar-Garcia, D. J. Payne, P. A. Hunt and K. R. J. Lovelock, *Phys. Chem. Chem. Phys.*, 2019, **21**, 18893-18910.
5. F. A. Cotton, M. Goodgame and D. M. Goodgame, *J. Am. Chem. Soc.*, 1961, **83**, 4690-4699.
6. M. Currie, J. Estager, P. Licence, S. Men, P. Nockemann, K. R. Seddon, M. Swadźba-Kwaśny and C. Terrade, *Inorg. Chem.*, 2013, **52**, 1710-1721.